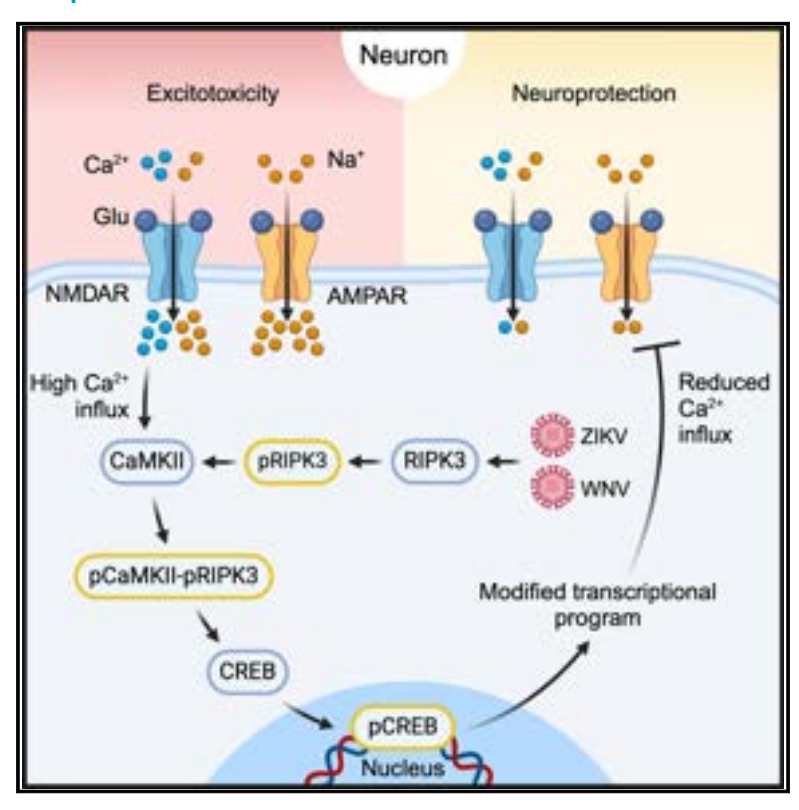
Immunity

The kinase RIPK3 promotes neuronal survival by suppressing excitatory neurotransmission during central nervous system viral infection

Graphical abstract



Authors

Irving Estevez, Benjamin D. Buckley, Marissa Lindman, ..., Colm Atkins, Bonnie L. Firestein, Brian P. Daniels

Correspondence

b.daniels@rutgers.edu

In brief

How innate immune signaling within neurons influences neurotransmission remains poorly understood. Estevez et al. show that the necroptotic kinase RIPK3 promotes neuronal survival during viral infections of the central nervous system by engaging a CaMKII/CREB-dependent transcriptional program that suppresses excitotoxic glutamate signaling. These findings highlight a mechanism of host protection driven by innate immune control of neurotransmission.

Highlights

- RIPK3 activation promotes neuronal survival during viral infections of the CNS
- RIPK3 suppresses excitotoxicity by dampening glutamatergic neurotransmission
- RIPK3-mediated neuroprotection is mediated via CaMKII/ CREB and is independent of MLKL







Article

The kinase RIPK3 promotes neuronal survival by suppressing excitatory neurotransmission during central nervous system viral infection

Irving Estevez, Benjamin D. Buckley, Marissa Lindman, Nicholas Panzera, Tsui-Wen Chou, Micheal McCourt, Brandon J. Vaglio, Colm Atkins, Bonnie L. Firestein, and Brian P. Daniels 2,*

¹Department of Cell Biology and Neuroscience, Rutgers University, Piscataway, NJ 08854, USA ²Lead contact

*Correspondence: b.daniels@rutgers.edu https://doi.org/10.1016/j.immuni.2025.01.017

SUMMARY

While recent work has identified roles for immune mediators in regulating neural activity, how innate immune signaling within neurons influences neurotransmission remains poorly understood. Emerging evidence suggests that the modulation of neurotransmission may serve important roles in host protection during infection of the central nervous system. Here, we showed that receptor-interacting protein kinase-3 (RIPK3) preserved neuronal survival during flavivirus infection through the suppression of excitatory neurotransmission. These effects occurred independently of the traditional functions of RIPK3 in promoting necroptosis and inflammatory transcription. Instead, RIPK3 promoted phosphorylation of the neuronal regulatory kinase calcium/calmodulin-dependent protein kinase II (CaMKII), which in turn activated the transcription factor cyclic AMP response element-binding protein (CREB) to drive a neuroprotective transcriptional program and suppress deleterious glutamatergic signaling. These findings identify an unexpected function for a canonical cell death protein in promoting neuronal survival during viral infection through the modulation of neuronal activity, highlighting mechanisms of neuroimmune crosstalk.

INTRODUCTION

While the field of neuroimmunology has historically focused on roles for immune signaling in driving the pathogenesis of neurological disorders, recent advances have refined our understanding of neuroimmune crosstalk to include indispensable roles for the immune system in nervous system development, homeostasis, and repair. Newly appreciated links between these two systems include roles for neuronal innate immune signaling in the regulation of neural activity. Within this context, immune mediators transcend their traditional functions in inflammation and pathogen control and become key players in the modulation of neural circuits, influencing processes ranging from neurotransmission to behavior. Defining the mechanisms and consequences of neuroimmune signaling has, therefore, become paramount to understanding the basic biology of the nervous system.

Recent work has described specialized adaptations of several innate immune processes in neurons. For example, we and others have described cell death-independent functions for receptor-interacting kinase-3 (RIPK3), the canonical inducer of a form of programmed cell death termed "necroptosis." ^{10–12} In the setting of neurotropic flavivirus infection, activation of RIPK3 does not engage the necroptotic executioner molecule mixed lineage kinase domain-like protein (MLKL) but rather coor-

dinates a shift in neuronal transcription to induce an antiviral state in the absence of cell death. ^{13–15} This outcome may represent an adaptive strategy to control infection without sacrificing a critical postmitotic cell type that cannot be replaced in the adult brain. ^{16,17} Despite these insights, the mechanisms by which RIPK3 shapes the neuronal transcriptome during infection are poorly understood, as are the ways in which engagement of this pathway influences neuronal cell biology beyond inducing antimicrobial gene expression.

Notably, aberrant neuronal activity appears to be a major driver of pathogenesis during viral infections of the central nervous system (CNS). 18-22 Perturbations to excitatory neurotransmission mediated by glutamate have been linked to the neurologic damage elicited by flaviviruses, including the major human pathogens West Nile virus (WNV), Zika virus (ZIKV), and Japanese encephalitis virus (JEV). 23-26 Flavivirus-induced enhancement of glutamate signaling results in excitotoxicity, a process triggered by the excessive activation of ionotropic glutamate receptors on neuronal cells. Excessive influx of calcium ions through the N-methyl-D-aspartate receptor (NMDAR), in particular, results in a cascade of events that culminates in neuronal damage and death.²⁷ While previous work has broadly identified roles for innate immune cytokines in sensitizing neurons to excitotoxicity, 28,29 the mechanisms by which viral infections shape neuronal excitability and, by extension,





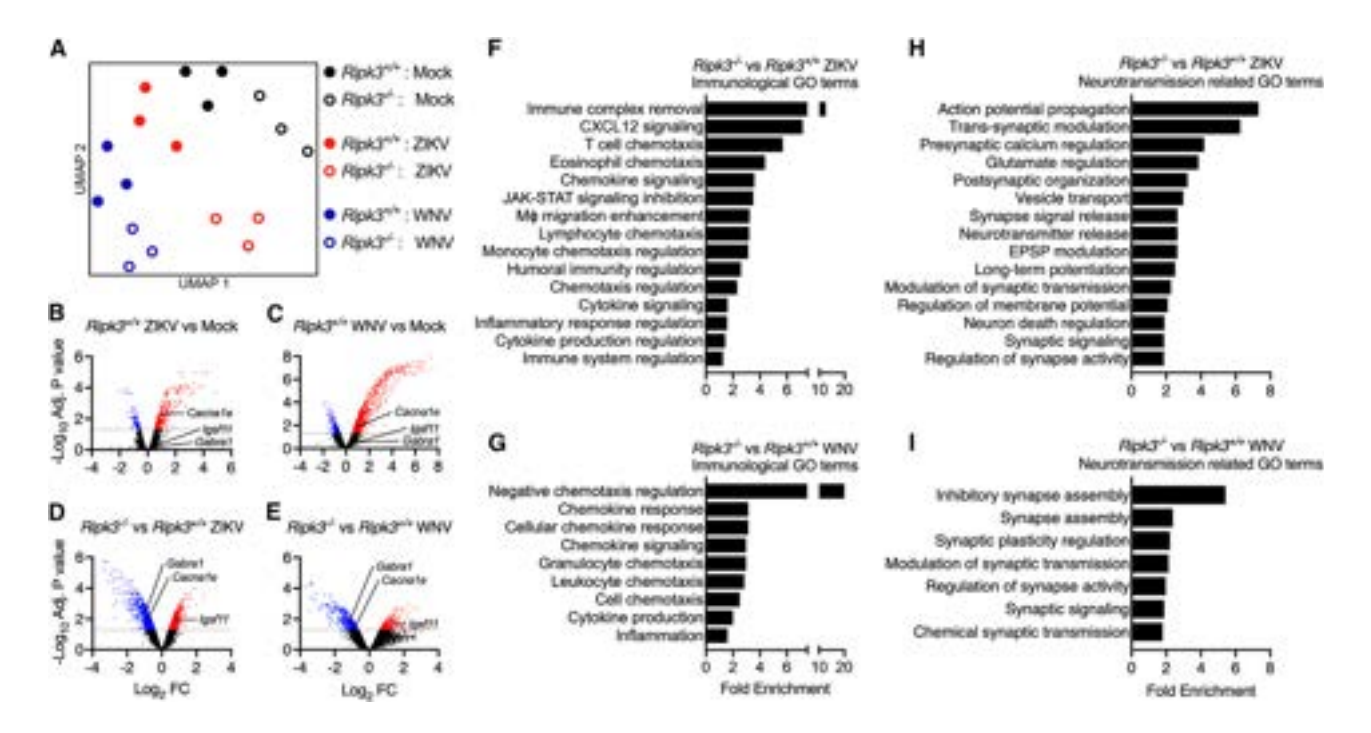


Figure 1. RIPK3 is a key regulator of neurologic gene expression during flavivirus infection

(A) Uniform manifold approximation and projection analysis of transcriptomic data from primary cortical neurons following 24 h infection with ZIKV or WNV. n = 3 independent cultures/condition.

(B–E) Volcano plots illustrating differential gene expression in neuronal cultures described in (A). Transcripts with significant changes (>1.5-fold change, adj. p < 0.05) are highlighted: downregulated transcripts are shown in blue and upregulated in red. Values in (B) and (C) represent values in WT (Ripk3*/+) neurons infected with ZIKV (B) or WNV (C) compared with uninfected WT control neurons. Values in (D) and (E) represent values in Ripk3*/- neuron cultures infected with ZIKV (D) or WNV (E) compared with Ripk3*/+ cultures infected with the same virus. Selected genes associated with neurotransmission are annotated. (F–I) Selected overrepresented GO terms obtained from GO enrichment analysis of DEGs between Ripk3*/- and Ripk3*/+ neurons infected with ZIKV or WNV, highlighting alterations in immunological (F and G) and neurological pathways (H and I). All terms were overrepresented with an FDR < 0.05.

susceptibility to excitotoxic cell death remain unclear. Such insight is critically needed as modulation of neuronal activity may represent an underexplored avenue of therapeutic development for neuroinvasive flavivirus infections, which are associated with a constellation of severe neurologic syndromes and for which there are currently no disease-specific treatments. 30,31

Here, we define an unexpected function for RIPK3 signaling in suppressing neuronal excitability during flavivirus infection, thereby promoting survival rather than cell death under excitotoxic conditions. Using both conditional Ripk3 deletion and an inducible chemogenetic RIPK3 activation system, we showed that RIPK3 activity in neurons suppressed sensitivity to glutamatergic stimulation, thereby promoting neuronal viability and host survival during both flavivirus infection and sterile excitotoxic insults. Mechanistically, we showed that the neuroprotective function of RIPK3 required the activity of calcium/calmodulindependent protein kinase II (CaMKII), which was phosphorylated in an RIPK3-dependent manner during flavivirus infection. This RIPK3/CaMKII axis activated the transcription factor cAMP response element-binding protein (CREB), which was also required for RIPK3-mediated suppression of excitotoxicity. We showed further that RIPK3-dependent engagement of CREB promoted the expression of a neuroprotective transcriptional program, identifying a mechanism of RIPK3-mediated transcriptional regulation in neurons that is independent of nuclear factor- κB (NF- κB)-dependent inflammatory gene expression or MLKL-dependent necroptosis. Together, these findings highlight mechanisms of neuroimmune crosstalk in which cell-intrinsic innate immune signaling in neurons can regulate fundamental, non-immune aspects of neuronal function, including neurotransmission.

RESULTS

RIPK3 is a key regulator of neurologic gene expression during flavivirus infection

To investigate how RIPK3 shapes neuronal responses to flavivirus infection, we performed secondary analysis of a transcriptomic dataset previously published by our group and others ¹³ in which primary cortical neuron cultures derived from Ripk3^{-/-} mice or wild-type (Ripk3^{+/+}) littermate controls were infected with either ZIKV-MR766 or WNV-TX02 for 24 h. Uniform manifold approximation and projection (UMAP) analysis revealed tight and distinct clustering that segregated samples by both genotype and infection status, suggesting clear RIPK3-dependent transcriptional responses to both viruses (Figure 1A). Further analysis revealed robust differential gene expression in Ripk3^{+/+} neurons in response to both ZIKV (Figure 1B) and WNV (Figure 1C), which was predominated by upregulated transcripts. Notably, Ripk3^{-/-} neurons exhibited hundreds of differentially expressed



genes (DEGs) compared with Ripk3+/+ controls following infection with both viruses (Figures 1D and 1E). Among these DEGs were key transcripts related to neurotransmission, including genes associated with α-amino-3-hydroxy-5-methyl-4-isoxazolepropionic acid receptor (AMPAR) trafficking (Igsf11), γ-aminobutyric acid (GABA) receptor subunits (Gabra1), and voltage-gated calcium channels (Cacna1e). Given this apparent role for RIPK3 in controlling genes involved in synaptic function, we performed Gene Ontology (GO) enrichment analysis to systematically profile the biological pathways impacted by RIPK3 during infection. GO enrichment analysis of significant DEGs revealed overrepresentation of terms related to immune activation when comparing Ripk3^{-/-} neurons to Ripk3^{+/+} controls in both infection groups (Figures 1F and 1G), consistent with our previous work demonstrating a central role for RIPK3 in promoting innate immune gene expression in neurons during flavivirus infection. 13-15 However, these comparisons also revealed enrichment of GO terms associated with neurologic functions, including terms such as synaptic signaling, long-term potentiation, and neurotransmitter release (Figures 1H, 1I, and S1). These data suggest that RIPK3 may shape features of neuronal cell biology that extend beyond inflammatory signaling during viral infection.

RIPK3 signaling during flavivirus infection promotes neuronal survival rather than cell death

Recent work has implicated glutamate-dependent excitotoxicity in promoting neuronal death during flavivirus infection. 20,25,32,3 We thus questioned whether the RIPK3-dependent neuronal transcriptional response included genes relevant for glutamate signaling. Ripk $3^{-/-}$ neurons indeed exhibited a complex pattern of up- and downregulated transcripts related to glutamate receptor signaling in both ZIKV and WNV infection groups (Figure 2A). To better understand the implications of these findings, we performed pathogenesis studies using pharmacologic agents that selectively antagonize the ionotropic glutamate receptors AMPAR and NMDAR, both of which mediate excitatory neurotransmission by facilitating postsynaptic cation influx (Figure 2B). We first assessed survival in immunocompetent mice following intracranial infection with ZIKV-MR766 (Figure 2C). We observed that Ripk3^{-/-} mice exhibited enhancement of clinical disease and mortality in this model (Figures 2D and S2A), consistent with our previous work. 13 However, this effect could be completely ameliorated via administration of the AMPAR antagonist GYKI 52466³⁴ (GYKI) daily on days 3–7 post infection. We performed similar experiments in mice harboring neuronspecific deletion of Ripk3 by crossing mice in which exons 2 and 3 of the endogenous Ripk3 locus are flanked by loxP sites³⁵ (Ripk3^{fl/fl}) to a line expressing Cre-recombinase under the control of the Synapsin-1 (Syn1) promoter. 36 Ripk3fl/fl Syn1 Cre+ mice also exhibited enhanced clinical disease and mortality following intracranial ZIKV or subcutaneous WNV infections compared with littermate controls, and this phenotype could also be ameliorated by treatment with GYKI (Figures 2E, 2F, S2B, and S2C), suggesting that antagonism of excitatory glutamatergic neurotransmission through AMPAR was sufficient to rescue the enhanced mortality resulting from loss of neuronal RIPK3. We observed similar results using the NMDAR antagonist MK801,³⁷ which rescued the enhanced disease burden and mortality observed in ZIKV-infected Ripk3^{-/-} mice (Figures 2G

and S2D) as well as ZIKV or WNV-infected Ripk3fl/fl Syn1 Cre+ mice (Figures 2H, 2I, S2E, and S2F). We also confirmed successful deletion of Ripk3 in neurons in Ripk3^{fl/fl} Syn1 Cre+ animals via fluorescent in situ hybridization (Figure S2G), further indicating the importance of neuronal RIPK3 signaling in these phenotypes. These findings support the idea that the enhanced viral pathogenesis observed in mice lacking neuronal RIPK3 is driven by excitotoxic glutamatergic neurotransmission.

To further test this idea, we assessed viability in primary cortical neuron cultures following ZIKV-MR766 infection using the MultiTox Cytotoxicity Assay, which simultaneously measures distinct protease activities associated with living and dead cells using fluorogenic peptide substrates.³⁸ Ripk3^{-/-} neurons exhibited diminished live-cell protease activity (AFC) and enhanced dead cell protease activity (R110) following ZIKV infection (Figure 2J), demonstrating that RIPK3 signaling promoted survival rather than cell death in this setting. GYKI treatment completely abrogated loss of viability in infected neurons in both assays, suggesting that the enhanced cell death occurring in the absence of RIPK3 was dependent on AMPAR-mediated glutamate signaling (Figure 2J). We observed essentially identical outcomes in experiments using the NMDAR antagonist MK801 (Figure 2K) and further confirmed these results using a traditional ATP-based viability assay (Figure S2H). Notably, we did not observe any impact of genotype or glutamate receptor blockade on brain viral burden in vivo (Figures S2I-S2L) or ZIKV replication in primary neuron cultures (Figure S2M), suggesting that the protective effects of these manipulations were not due to direct suppression of viral replication.

We next questioned the manner in which neurons die following flavivirus infection. Inhibition of the apoptotic effectors caspase 3 and caspase 7 with Z-DEVD prevented loss of viability at 24 h post-ZIKV infection in wild-type neuron cultures (Figure S2N). By contrast, inhibition of the pyroptosis effector caspase 1 with Ac-YVAD did not impact neuronal cell death following ZIKV infection. Additionally, inhibition of RIPK3 with GSK872 resulted in enhanced neuronal cell death following infection, and this effect was prevented by treatment with Z-DEVD but not by Ac-YVAD. We also observed increased caspase 3 activity following infection, which was further increased by RIPK3 inhibition with GSK872 (Figure S2O), confirming that RIPK3 restrains neuronal apoptosis during ZIKV infection. Notably, pretreatment with MK801 prevented engagement of caspase 3 activity, further suggesting that neuronal apoptosis during ZIKV infection is primarily driven by NMDAR-dependent excitotoxicity. We also confirmed that, while ZIKV induced enhanced glutamate release in cultured neurons (consistent with previous reports³²), this effect did not differ between Ripk3^{+/+} and Ripk3^{-/-} cultures (Figure S2P), suggesting that differences in survival were not driven by differential glutamate release into culture media. Furthermore, we did not observe differences between genotypes following sterile exposure to varying concentrations of exogenous glutamate or NMDA, indicating that Ripk3 deficiency alone does not alter baseline sensitivity to glutamate- or NMDA-induced toxicity (Figures S2Q and S2R). Collectively, these results support the idea that flavivirus infection induces neuronal apoptosis via glutamatergic excitotoxicity and that neuronal RIPK3 signaling suppresses this effect.



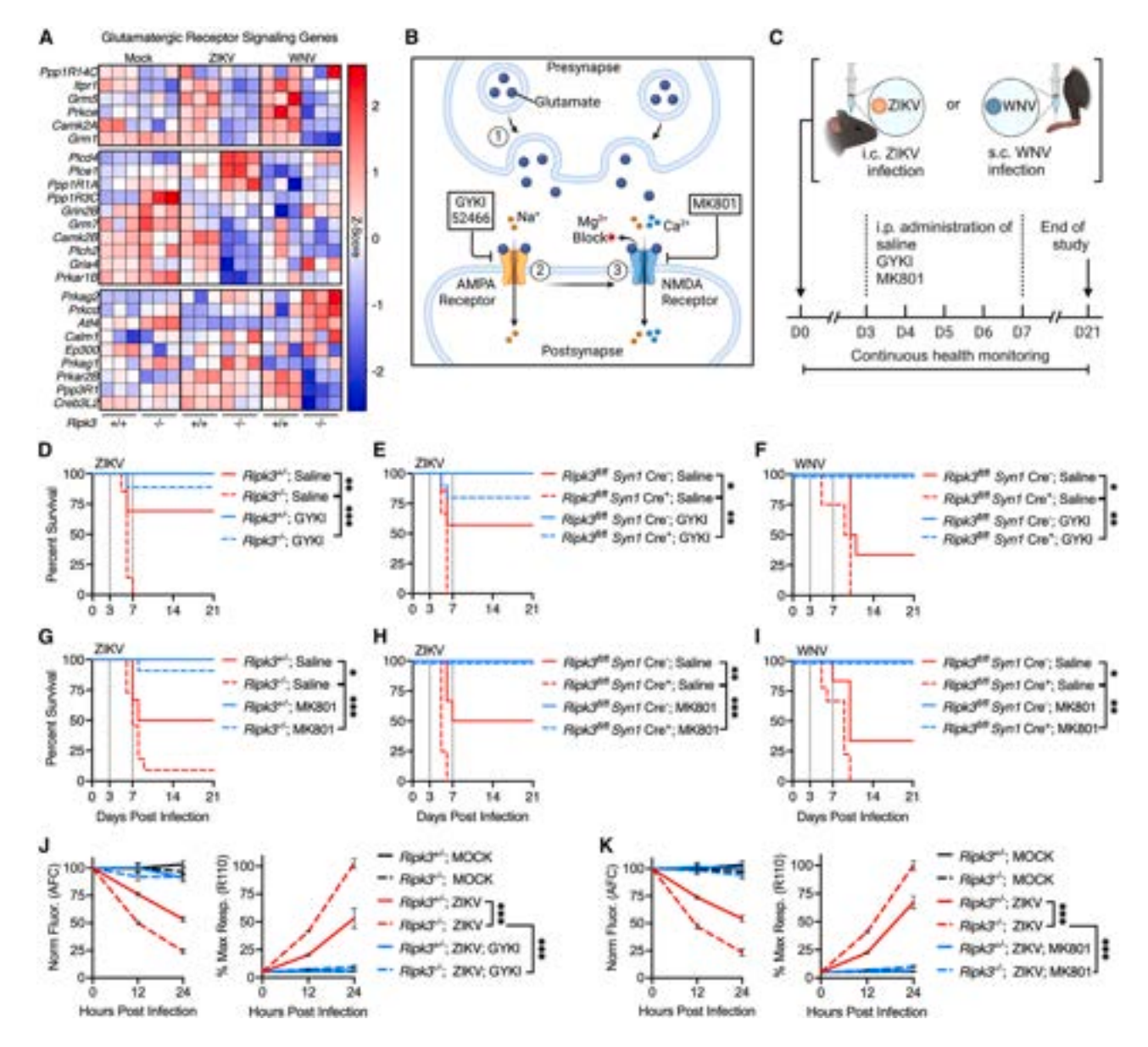


Figure 2. RIPK3 signaling during flavivirus infection promotes neuronal survival rather than cell death

(A) Heatmap depicting selected glutamatergic receptor signaling-associated genes derived from microarray profiling of primary cortical neurons following 24 h infection with ZIKV or WNV.

(B) Schematic representation of glutamatergic signaling and inhibitors used in our study. Note sequential influx of Na⁺ through AMPA receptors (blocked by GYKI-52466) and Na⁺/Ca2⁺ through NMDA receptors (blocked by MK801).

(C) Schematic representation of survival studies in which mice underwent either intracranial ZIKV or subcutaneous WNV infections. Animals were treated with either saline, GYKI-52466 (1 μg/g), or MK801 (0.06 μg/g) on days 3–7 post infection.

(D–I) Survival analysis in mice following ZIKV or WNV infection with or without 5 daily treatments using GYKI-52466 (D–F) or MK801 (G–I). n = 6-13 mice per genotype for ZIKV studies and N = 4-9 for WNV studies. All values are pooled from 2–3 independent experiments.

(J and K) MultiTox cell death assays: Live (AFC) and dead (R110) protease activities were measured in primary neuron cultures infected with ZIKV following pretreatment with GYKI-52466 (J) or MK801 (K). Fluorescence for AFC is normalized to mock controls, and the percentage of maximum R110 response is normalized to the group exhibiting the highest signal intensity at 24 h. n = 6 independent cultures per group/condition pooled from 2 independent experiments. **p < 0.01, ***p < 0.001. Error bars represent SEM. See also Figure S2.

RIPK3 modulates neuronal excitability and promotes neuroprotection during excitotoxicity

Previous work has shown that glutamate-induced excitotoxicity is initiated by an overabundance of intracellular Ca²⁺ ions that

drive neuronal cell death.^{39–41} Increased cytoplasmic Ca²⁺ influx via NMDARs has also been shown to drive neuronal cell death during viral infection.³² We therefore questioned whether prophylactic engagement of RIPK3 could suppress neuronal cell



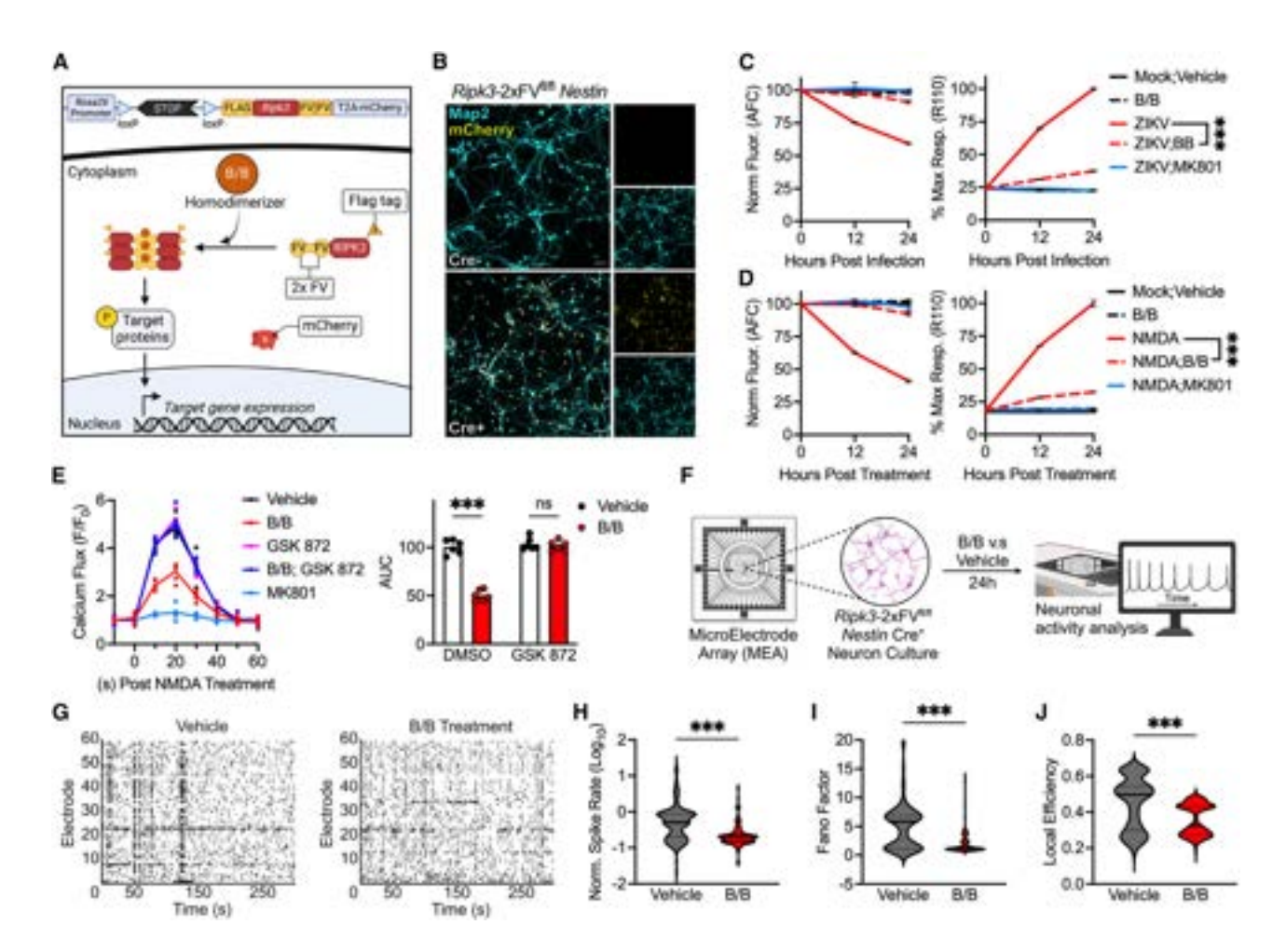


Figure 3. RIPK3 modulates neuronal excitability and promotes neuroprotection during excitotoxicity

(A) Schematic of the Ripk3-2xFV^{fl/fl} activation system. Transgene expression is controlled by a lox-STOP-lox element and is coupled with a non-fused mCherry reporter. Treatment with B/B induces FV-mediated dimerization, activating RIPK3, which triggers subsequent protein phosphorylation and gene expression. (B) Immunocytochemistry in primary neuron cultures displaying neuronal MAP2 (cyan) and mCherry (yellow) staining. Scale bar: 50 μm. (C and D) MultiTox cell viability assay in Ripk3-2xFV^{fl/fl} Nestin Cre+ neurons pretreated for 24 h with B/B, followed by exposure to ZIKV (C) or NMDA (D). Panels report live (AFC) and dead (R110) protease activity, as indicated. n = 6 independent cultures per group/condition pooled from 2 independent experiments. (E) NMDA-evoked Ca²⁺ dynamics in cortical neuron cultures following 24 h pretreatment with specified drugs, measured at 10-second intervals in the presence of Brilliant Calcium Flex reagent. Right panel displays area under the curve (AUC) analysis. n = 6 independent cultures per group/condition pooled from 2 independent experiments.

(F–J) Primary neurons from Ripk3-2xFV^{fl/fl} Nestin Cre⁺ mice were cultured on microelectrode arrays. Following 24 h treatment with either B/B or vehicle, neuronal activity on individual arrays was recorded and analyzed (F). Representative raster plots displaying activity across individual electrodes over time are shown (G), with quantitative analysis of normalized spike rates (H), Fano factor (I), and local network efficiency (J). n = 3 arrays per group, with each array containing 59 recording electrodes.***p < 0.001. Error bars represent SEM. See also Figure S3.

death during excitotoxic stimulation. We thus generated primary cortical neuron cultures from mice expressing a chemogenetically activatable form of RIPK3 (RIPK3-2xFV)14 under the control of the Nestin promoter (Ripk3-2xFV^{fl/fl} Nestin Cre+). RIPK3-2xFV proteins contain tandem FK506-binding protein (FKBP)F36V domains that drive forced oligomerization and activation of RIPK3 following exposure to the dimerization drug B/B homodimerizer (B/B) (Figure 3A). Using this system, we can induce sterile activation of RIPK3 in the absence of any exogenous stimulus. We validated the expression of RIPK3-2xFV by confirming the expression of the reporter mCherry (Figures 3B and S3A) and the induced expression of Cxcl10 (Figure S3B), which is strongly

induced by RIPK3 in a variety of settings. 13,14,42 We pretreated RIPK3-2xFV-expressing neuron cultures with B/B for 24 h, followed by infection with ZIKV-MR766 and assessment of cell viability. B/B pretreatment robustly suppressed cell death induced by ZIKV infection, further supporting a pro-survival function of this molecule in neurons (Figure 3C). B/B pretreatment also protected neurons from an excitotoxic dose of exogenous NMDA, confirming that RIPK3 can directly impact the cellular outcomes of glutamatergic receptor activation (Figure 3D). We repeated these experiments using an alternative ATP-based viability assay, confirming that B/B pretreatment was neuroprotective against both ZIKV and NMDA insults in Ripk3-2xFV^{fI/fI}



Nestin Cre+ neurons but not in Cre- cultures that lack RIPK3-2xFV transgene expression (Figures S3C and S3D).

We next evaluated whether RIPK3 activation could modulate NMDAR-dependent Ca2+ flux. We measured intracellular Ca2+ dynamics following a pulse stimulation with NMDA in neurons expressing RIPK3-2xFV using a cell-permeable fluorometric indicator (Brilliant Calcium). While vehicle-treated neurons exhibited robust calcium flux in response to NMDA, this response was diminished in neurons pretreated for 24 h with B/B (Figure 3E). This suppressive effect could be completely abolished in the presence of a pharmacologic inhibitor of RIPK3 kinase activity (GSK872), suggesting that RIPK3 kinase function was required for this activity. Importantly, the effect of GSK872 did not arise due to drug-induced changes in neuronal viability (Figure S3E). Calcium flux in this assay could also be completely abolished in the presence of MK801, confirming that we were measuring NMDAR-dependent activity. Notably, we observed that a short 2 h pretreatment with B/B failed to suppress NMDA-induced calcium flux, suggesting that this effect likely does not occur via immediate RIPK3-mediated regulation of NMDAR function but instead requires engagement of downstream signals that require more time to impact neuronal calcium dynamics (Figure S3F). Together, these results indicate that RIPK3 kinase activity is capable of suppressing NMDAR-dependent Ca²⁺ flux in neurons.

To further establish whether RIPK3 activation could directly impact neurotransmission, we cultured Ripk3-2xFV^{fl/fl} Nestin Cre+ neurons on microelectrode arrays (MEAs) and recorded spontaneous network activity following 24 h treatment with either B/B or vehicle control solution (Figure 3F). Notably, B/Btreated cultures displayed a reduction in spontaneous spiking activity (Figures 3G and 3H), suggesting a decrease in overall neuronal excitability. Furthermore, spiking activity in B/B-treated cultures exhibited less variability over time as quantified by the Fano factor statistic (Figure 3I), indicating an overall decrease in the complexity of spike activity within the neural network. We also observed a decrease in local efficiency of signal transmission in cultures treated with B/B (Figure 3J), consistent with an overall diminishment of signal propagation and network connectivity. These findings further support the idea that RIPK3 activation directly modulates neurotransmission by dampening synaptic activity, which may represent a mechanism of neuroprotection under excitotoxic conditions.

RIPK3 activation modulates neural activity in vivo during flavivirus infection

To explore potential links between RIPK3 function and neural excitability, we returned to our transcriptomic analysis of primary neurons and performed ingenuity pathway analysis⁴³ (IPA) to assess how RIPK3 expression influenced the representation of "disease and function" terms related to neurotransmission. We observed enhanced activation scores for many neurologic disease terms in Ripk3^{-/-} neurons infected with either ZIKV or WNV (Figure 4A). Notably, terms related to disordered neural activity, such as seizure and epilepsy, were particularly enriched in Ripk3^{-/-} neurons following ZIKV infection, while other terms, such as locomotion and movement disorders, were enriched for both viruses. Further analysis revealed hundreds of DEGs related to the seizure and epilepsy-associated IPA terms in Ripk3^{-/-} neurons following infection with both viruses (Figure 4B; Table S1), suggesting that RIPK3 modulates a broad program of genes related to neural excitation during flavivirus infection.

We next explored whether RIPK3 influences neuronal activity during flavivirus infection in vivo using an established model of chemically induced seizure in which mice are injected with pentylenetetrazol⁴⁴ (PTZ), a GABA type A receptor antagonist. Following intracranial ZIKV infection, mice were subjected to PTZ administration, and seizure severity was recorded using a modified Racine scale⁴⁵ (Figure 4C). We did not observe a significant effect of genotype in mock-infected control groups; however, infected Ripk3^{-/-} mice demonstrated a significant increase in seizure severity compared with infected littermate controls, both in terms of the overall distribution of scores within genotypes as well as the total proportion of mice reaching a "severe" score of 4 or greater on the Racine scale (Figure 4D). Identical experiments in neuron-specific Ripk3 knockout mice revealed similar results (Figure 4E). Notably, infected mice with intact Ripk3 exhibited reduced seizure severity compared with their mock-infected counterparts, consistent with the idea that engagement of RIPK3 during infection suppresses neuronal excitation. We also observed that infected Ripk3 $^{-/-}$ and Ripk3 $^{fl/fl}$ Syn1 Cre+ mice exhibited reduced latencies in reaching successive stages along the seizure severity scale (Figures 4F and 4G), while we did not detect genotype-dependent changes in seizure latency in mock-infected groups (Figures S4A and S4B). Similar experiments revealed no significant differences in PTZ-induced seizure susceptibility between Mlkl-/- mice and Mlkl+/- littermate controls following infection (Figures S4C-S4E), suggesting that RIPK3-mediated suppression of seizure severity was independent of MLKL-dependent mechanisms such as necroptosis, in line with our previous work. 13-15 Together, these data show that RIPK3 activity within the infected CNS can suppress aberrant neural excitation in vivo.

RIPK3 signaling drives activation of the key neural regulatory kinase CaMKII

We next sought to define downstream signaling mechanisms by which RIPK3 modulates neuronal excitability. IPA of kinase networks putatively engaged by RIPK3 in primary neurons revealed diminished activation of gene networks regulated by many immunological kinases, including janus kinase (JAK) 1/2, IκB kinase (IKK), and TANK-binding kinase 1 (TBK1), in Ripk3^{-/-} neurons following both ZIKV and WNV infection (Figure 5A), consistent with established roles for RIPK3 in driving transcription of inflammatory genes. However, we also noted that loss of RIPK3 signaling was associated with diminished activation of genes controlled by CaMKII. This molecule represented an attractive mechanistic candidate in our study, as CaMKII, and the CaMKIIa isoform in particular, is a well-established modulator of a diverse array of processes related to neurotransmission, including glutamate receptor signaling, long-term potentiation, and survival following neurotoxic insults. 46,47 Recent work also suggested that CaMKII may be a substrate of RIPK3 in cardiomyocytes. 48 To test whether RIPK3 activation leads to CaMKIIα activation in neurons, we infected Ripk3^{fl/fl} Syn1 Cre+ mice or Cre- controls with ZIKV and performed immunohistochemistry on day 4 post infection, which revealed an increase in neuronal pCaMKII (p-Thr286) signal intensity in the cerebral



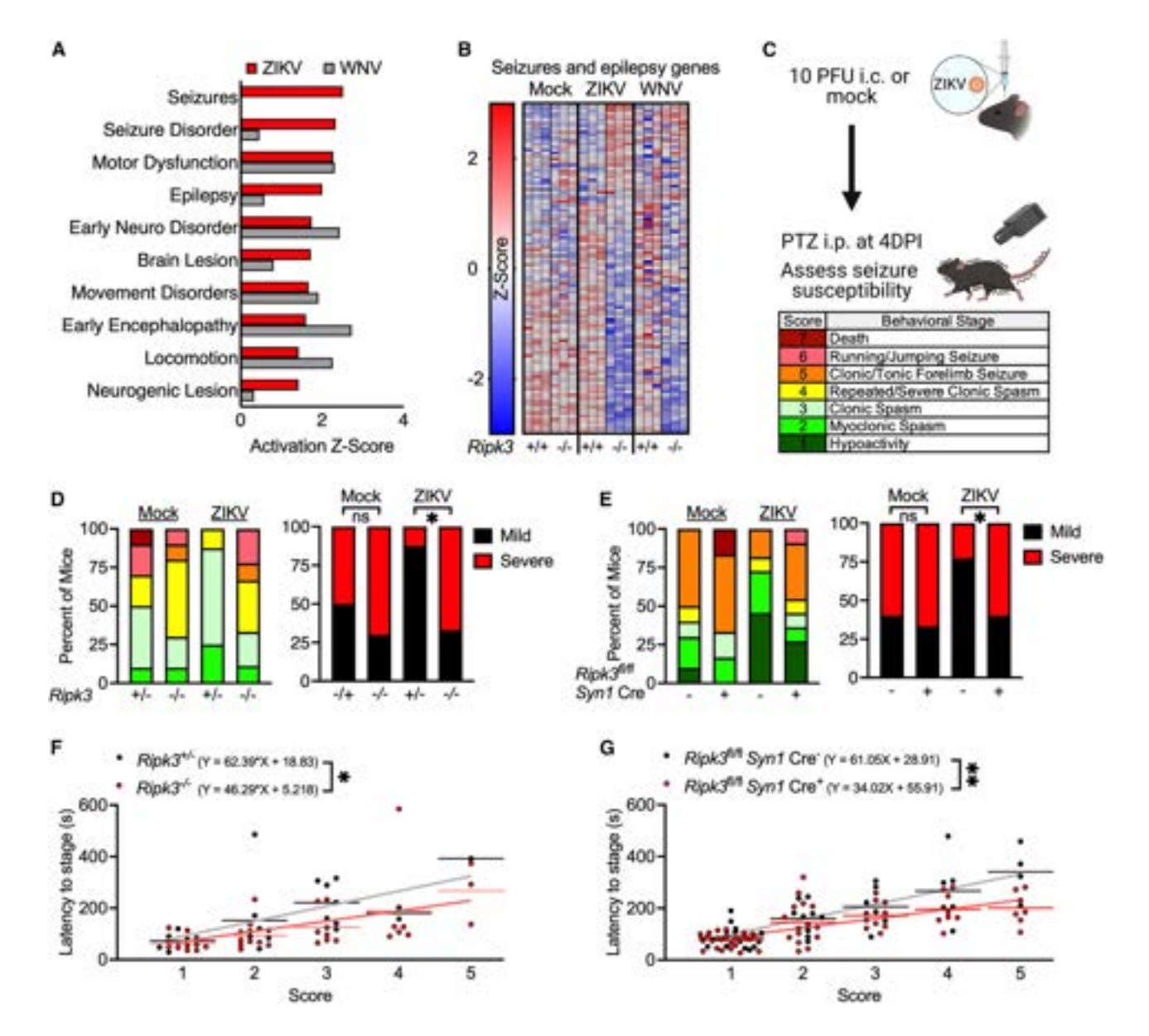


Figure 4. RIPK3 activation modulates neural activity in vivo during flavivirus infection

- (A) Ingenuity pathway analysis of significant DEGs derived from microarray profiling of primary neurons after 24 h infection with ZIKV or WNV.
- (B) Heatmap showing selected DEGs associated with seizures and epilepsy. This gene set was generated using ingenuity pathway analysis based on the disease and function terms identified in (A).
- (C) Schematic depicting the protocol for inducing seizures with pentylenetetrazol (PTZ) 4 days after intracranial ZIKV infection, including a table explaining the modified Racine scale of murine seizure stages.
- (D and E) Proportion of mice reaching indicated behavioral seizure stages, with "severe" seizures defined as stage 4 or higher. n = 8-10 (D) or 10-22 (E) mice per group. All data are pooled from 2-3 independent experiments.

(F and G) Latency time in seconds for infected mice to reach consecutive seizure stages as shown in (D) and (E). Linear regression was used to compare overall rates of seizure progression between groups. Latency calculations end at stage 5 as proportionally too few control mice reach higher stages to include in the regression analysis.*p < 0.05, **p < 0.01.

See also Figure S4.

cortex of Cre- animals that was reduced in Cre+ mice lacking neuronal Ripk3 (Figure 5B). By contrast, we did not observe differences in pCaMKII signal intensity between genotypes in mock-infected mice. We also performed in vivo negative selection purification of neurons from ZIKV-infected mice using magnetic activated cell sorting (MACS) (Figure 5C). CaMKII activity was robustly enhanced in sorted neurons from infected Cremice, while this effect was diminished in neuron-specific Ripk3 knockout mice (Figure 5D). We also observed enhanced CaMKII activity in Ripk3^{+/-} but not Ripk3^{-/-} primary cortical neurons infected with ZIKV, an effect that was also prevented by treatment with the CaMKII inhibitor KN93 (Figure 5E). These



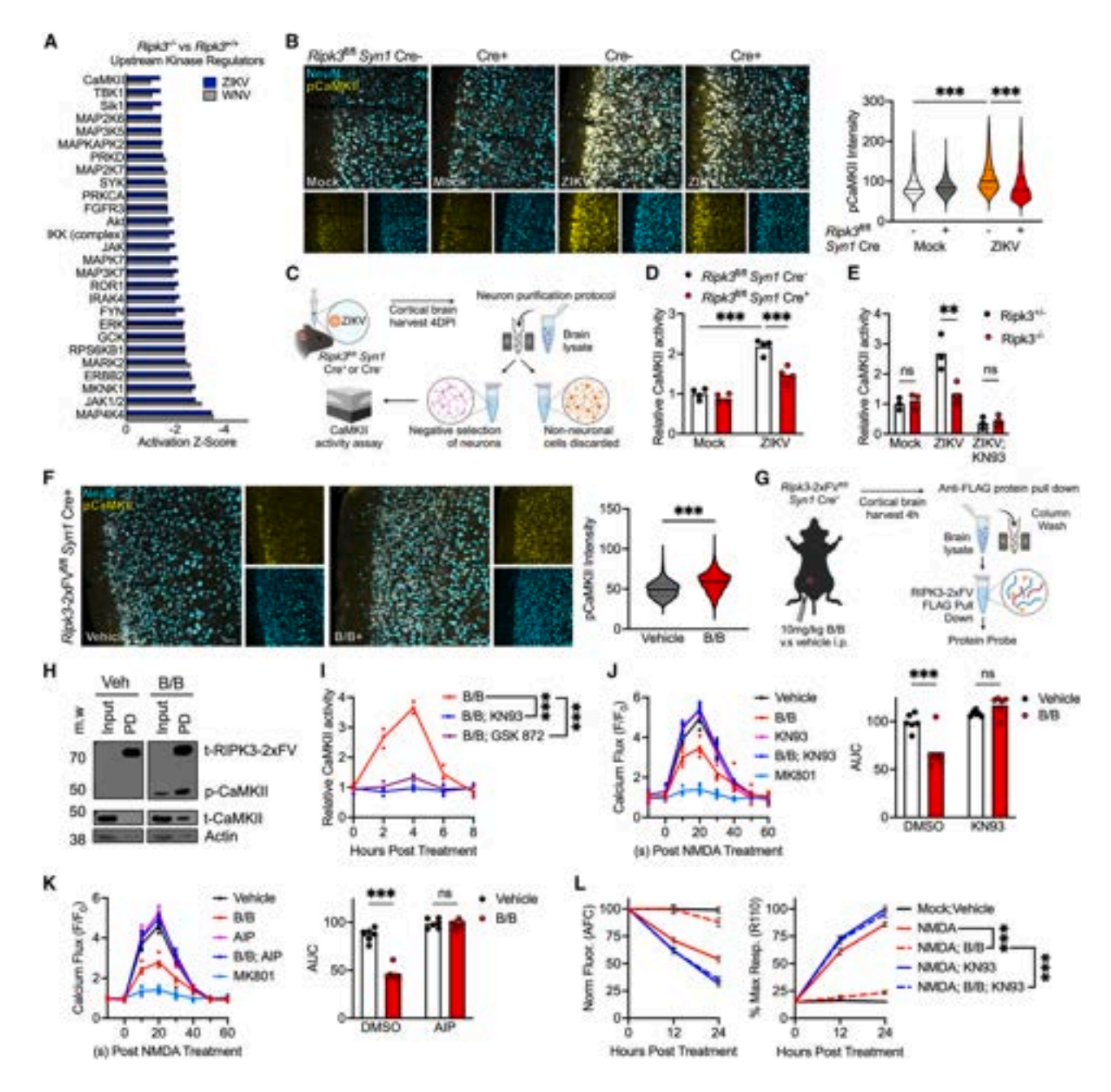


Figure 5. RIPK3 signaling drives activation of the key neural regulatory kinase CaMKII

(A) Ingenuity pathway analysis comparing kinase network activation in neurons infected with ZIKV or WNV.

(B) Immunohistochemistry on cortical brain tissue 4 days after intracranial ZIKV infection, with staining for NeuN (cyan) and p-Thr286 CaMKII (yellow). Colocalized pCaMKII signal intensity in NeuN+ cells was measured using QuPath software. n = 6 mice per genotype/condition pooled from 2 independent experiments. Scale bar: 50 μm.

(C and D) Schematic of the negative selection MACS protocol used to purify neurons from cerebral cortices 4 days following ZIKV infection (C). (D) Shows ELISAbased detection of CaMKII activity in isolated cortical neurons.

- (E) ELISA-based assay of CaMKII activity in primary cortical neuron cultures 24 h post-ZIKV infection.
- (F) Immunohistochemistry on cortical brain tissue as described in (B) 4 h post vehicle or B/B treatment. n = 6 mice per treatment pooled from 2 independent experiments. Scale bar: 50 µm.
- (G) Schematic illustrating the pulldown assay of FLAG-tagged RIPK3-2xFV protein from cortical brain tissue derived from Ripk3-2xFV^{fl/fl} Syn1 Cre+ mice, 4 h after B/B administration.
- (H) Western blot analysis of phosphorylated (p)-CaMKII in the input and pulldown (PD) samples, with total (t)-CaMKII, p-CaMKII, and RIPK3 shown for comparison. Actin is used as a loading control. Blots are representative of 3 independent experiments.
- (I) ELISA-based assay of CaMKII activity in Ripk3-2xFV^{fl/fl} Nestin Cre⁺ primary cortical neuron cultures at indicated time points following treatment with B/B.



data suggest that ZIKV infection in neurons engages the phosphorylation of CaMKII in a RIPK3-dependent manner.

We also performed complementary experiments using our chemogenetic system to selectively activate neuronal RIPK3 in the absence of infection. We generated mice expressing the activatable RIPK3-2xFV protein under the Syn1 promoter (Ripk3-2xFV^{fl/fl} Syn1 Cre⁺) and confirmed neuron-specific expression of the construct (Figure S5A). These mice were treated with B/B or vehicle solution for 4 h, which resulted in a significant increase in neuronal pCaMKII signal intensity in B/B-treated animals but not vehicle-treated controls (Figure 5F). We next leveraged the FLAG tag on the chimeric RIPK3-2xFV protein to investigate potential interactions between RIPK3 and CaMKII. We treated Ripk3-2xFV^{fl/fl} Syn1 Cre+ mice with B/B for 4 h then harvested cerebral cortices and performed protein pulldown of RIPK3-2xFV using beads coated with anti-FLAG antibodies (Figure 5G). Western blot confirmed the expression of the RIPK3-2xFV protein as well as highly efficient pulldown in both treatment groups (Figures 5H and S5B). Notably, we again observed that chemogenetic activation of RIPK3 induced CaMKIIa activation, as evidenced by detection of p-CaMKIIa following B/B treatment. Moreover, we observed substantial pulldown of RIPK3-2xFV with both total and phosphorylated CaMKIIα when RIPK3 activation was enforced with B/B, suggesting that CaMKIIa may be a direct substrate of RIPK3 kinase activity, or that the proteins interact indirectly in a complex that ultimately drives CaMKIIa phosphorylation. To further test this idea, we assessed CaMKII activity following sterile RIPK3 activation with B/B in Ripk3-2xFV^{fl/fl} Nestin Cre+ primary neuron cultures. We observed a time-dependent increase in CaMKII activity that peaked 4 h following B/B administration (Figure 5I) and was abolished by co-treatment with the CaMKII inhibitor KN93 or GSK872, suggesting that RIPK3 kinase activity is required to drive CaMKII activation in this setting.

We also assessed whether engagement of CaMKII was required for RIPK3-dependent modulation of neuronal physiology. We first assessed calcium flux dynamics by treating Ripk3-2xFV^{fl/fl} Nestin Cre+ neuron cultures overnight with B/B in the presence of either of two CaMKII inhibitors, including KN93 and a cell-permeable CaMKII-specific inhibitory peptide (AIP), which were used at concentrations that did not impact neuronal viability (Figure S5C). Inhibition of CaMKII activity with either reagent prevented suppression of calcium flux in B/Btreated neurons (Figures 5J and 5K). We also evaluated NMDA-induced excitotoxicity in Ripk3-2xFV^{fl/fl} Nestin Cre+ neurons pretreated with B/B with or without KN93 using the MultiTox Cytotoxicity Assay, observing that pharmacologic inhibition of CaMKII abrogated the pro-survival effect of enforced RIPK3 activation (Figure 5L). Together, these data suggest that CaMKII is required for the neuroprotective functional outcomes of RIPK3 activation in neurons.

RIPK3/CaMKII signaling promotes neuroprotection through engagement of CREB and *de novo* transcription

To better understand how RIPK3/CaMKII signaling axis promotes neuroprotection against excitotoxicity, we next interrogated how this pathway shapes neuronal gene expression. Notably, CaMKII is known to influence neural physiology in large part through its activation of the transcription factor CREB. 49,50 CREB phosphorylation at Ser133 by CaMKII initiates a transcriptional response that promotes neuroprotection subsequent to NMDAR activation. 27,51 We therefore hypothesized that RIPK3-CaMKII signaling culminates in CREB-mediated transcriptional responses. To test this idea, we performed immunohistochemical staining for p-Ser133 CREB (pCREB) 4 days following intracranial ZIKV infection. We observed a significant increase in neuronal pCREB signal intensity in the cerebral cortices of control mice following ZIKV infection, which was diminished in mice lacking neuronal RIPK3 (Figure 6A). By contrast, no differences in pCREB signal intensity were observed between genotypes in mock-infected animals. We also assessed CREB activation using an ELISA-based assay in which phosphorylated CREB is captured on plates coated with the cAMP response element DNA sequence, enabling colorimetric detection (Figure 6B). This assay revealed enhanced CREB phosphorylation in magnetically sorted neurons from ZIKV-infected control mice but not those lacking neuronal RIPK3 (Figure 6C). Further experiments showed that ZIKV infection also resulted in enhanced CREB phosphorylation in Ripk3^{+/-} but not Ripk3^{-/-} cortical neuron cultures and that ZIKV-induced CREB phosphorylation was prevented in the presence of KN93 (Figure 6D). We similarly observed diminished activation of CREB in infected neurons treated with GSK872 (Figure S6A), as well as in neurons in which Camk2a or Creb1 were knocked down using small interfering RNA (siRNA) (Figure S6B), suggesting that ZIKV infection drives neuronal CREB activation in a manner that requires the kinase activities of both RIPK3 and CaMKII. We also confirmed that siRNA knockdown of Camk2a or Creb1 was sufficient to exacerbate neuronal cell death following ZIKV infection (Figure S6C). Complementary experiments revealed that sterile chemogenetic activation of RIPK3 could also induce neuronal CREB phosphorylation in littermate control mice but not in those lacking neuronal RIPK3 (Figure 6E). In vitro experiments using Ripk3-2xFV^{fl/fl} Nestin Cre+ cortical neuron cultures also showed that B/B treatment resulted in enhanced CREB activation (Figure 6F) that was abolished in the presence of GSK872 or KN93. Together, these data strongly suggest a signaling pathway in which RIPK3 drives successive signaling events involving CaMKII activation followed by CREB activation in neurons.

We thus next explored the role of CREB in modulating RIPK3/CaMKII-mediated calcium flux after NMDA pulse stimulation. We observed that the CREB inhibitor 666-15 abrogated the suppressive effect of B/B treatment on neuronal calcium flux in response

⁽J and K) NMDA-evoked Ca^{2+} dynamics in cortical neuron cultures following 24 h pretreatment with specified drugs, measured at 10-second intervals in the presence of Brilliant Calcium Flex reagent. Right panel displays AUC analysis. n = 6 independent cultures per group/condition pooled from 2 independent experiments.

⁽L) MultiTox cell viability assay in Ripk3- $2xFV^{fl/fl}$ Nestin Cre⁺ neurons treated with B/B homodimerizer for 24 h, followed by exposure to NMDA. Panels report live (AFC) and dead (R110) protease activity. n = 6 independent cultures per group/condition pooled from 2 independent experiments. **p < 0.001, ***p < 0.001. Error bars represent SEM.



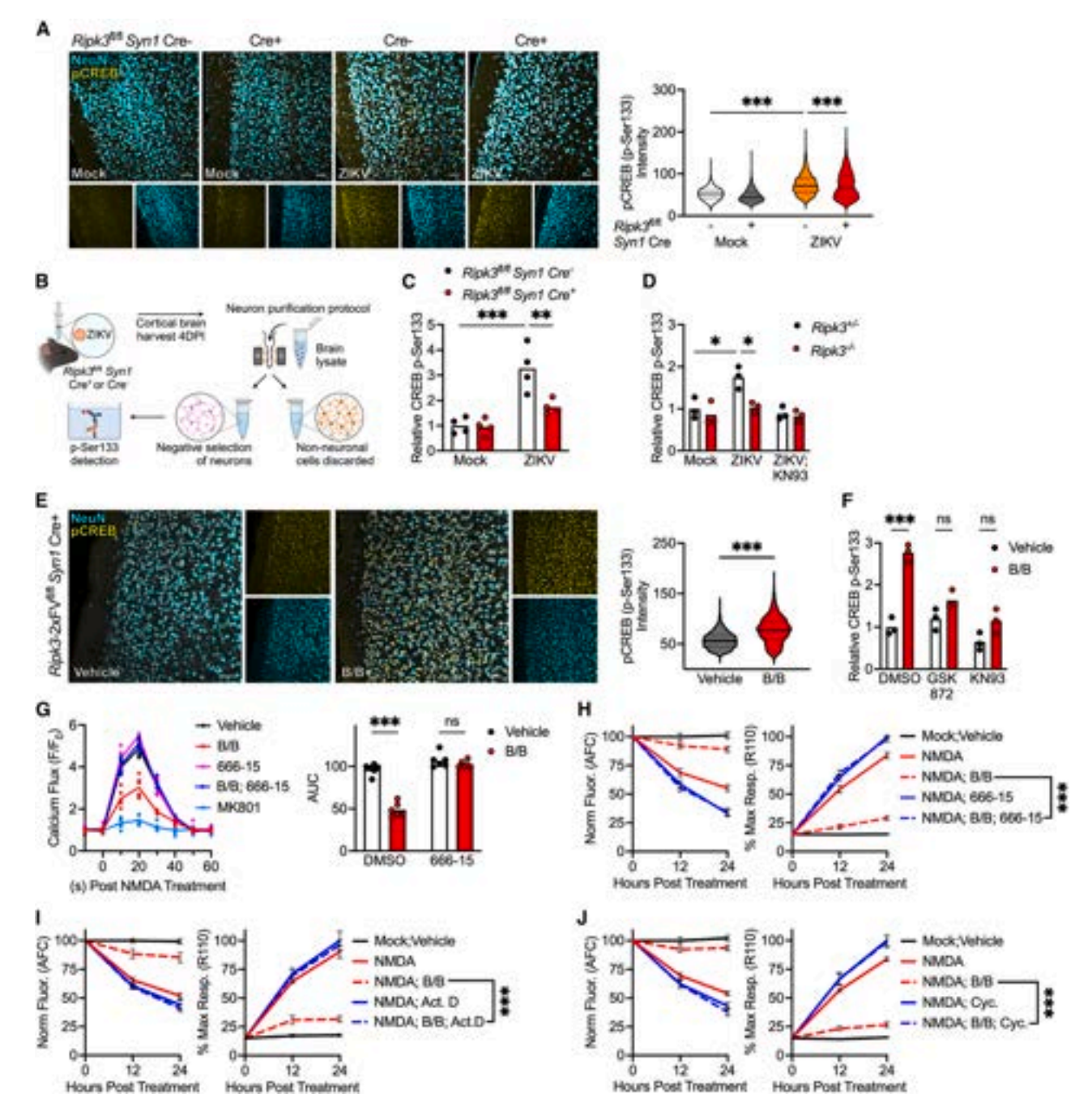


Figure 6. RIPK3/CaMKII signaling promotes neuroprotection through engagement of CREB and de novo transcription

(A) Immunohistochemistry on cortical brain tissue 4 days post intracranial ZIKV infection, with staining for NeuN (cyan) and phospho p-Ser133 CREB (yellow). Colocalized pCREB signal intensity in NeuN+ cells was measured using QuPath software. n = 6 mice per genotype/condition pooled from 2 independent experiments. Scale bar: 50 µm.

- (B and C) Schematic of the negative selection MACS protocol used to purify neurons from cerebral cortices 4 days following ZIKV infection (C).
- (D) ELISA detection of pCREB in cortical neuron cultures 24 h following ZIKV infection. n = 3 independent cultures per genotype/condition.
- (E) Immunohistochemistry on cortical brain tissue as described in (A) 4 h post B/B treatment. n = 6 mice per treatment pooled from 2 independent experiments. Scale bar: 50 µm.
- (F) Detection of pCREB in Ripk3-2xFV^{fl/fl} Nestin Cre⁺ neuron cultures 4 h following treatment with B/B and specified inhibitors. n = 3 independent cultures per
- (G) NMDA-evoked Ca2+ dynamics in cortical neuron cultures following 24 h pretreatment with specified drugs, measured at 10-second intervals in the presence of Brilliant Calcium Flex reagent. Right panel displays AUC analysis. n = 6 independent cultures per group/condition pooled from 2 independent experiments.



to NMDA, suggesting that CREB-mediated transcription is required for this effect (Figure 6G). By contrast, neither of the two inhibitors of nuclear factor κB (NF-κB) influenced RIPK3mediated suppression of neuronal calcium flux (Figures S6D and S6E), suggesting that modulation of neurotransmission is likely not a nonspecific effect of RIPK3-dependent inflammatory activation in neurons. We also observed that blockade of CREB activation with 666-15 prevented the neuroprotective effect of RIPK3 activation in RIPK3-2xFV expressing neuron cultures following exposure to a toxic NMDA stimulus (Figures 6H and S6F). To more firmly establish whether RIPK3-mediated neuroprotection required de novo transcription and translation, we performed cell viability experiments in which RIPK3 was chemogenetically activated in the presence of the transcription inhibitor actinomycin D or the translation inhibitor cycloheximide at concentrations that were not intrinsically toxic to cultured neurons (Figure S6G). These experiments showed that inhibition of either process abrogated the ability of RIPK3 activation to suppress NMDA-induced neuronal cell death (Figures 6I and 6J). Together, these data support a model in which RIPK3 preserves neuronal survival through engagement of CaMKII-dependent activation of CREB, which induces expression of transcriptional targets that promote neuroprotection during excitotoxic insults.

RIPK3 activation induces a CaMKII- and CREBdependent neuroprotective transcriptional program

To further assess how the RIPK3/CaMKII/CREB pathway influences neuronal transcription, we performed bulk RNA sequencing (RNA-seq) of primary cortical neuron cultures expressing RIPK3-2xFV treated for 24 h with B/B or ethanol vehicle in the presence of KN93, 666-15, or DMSO vehicle. Chemogenetic activation of RIPK3 robustly altered the neuronal transcriptome, as indicated by 6,313 significant DEGs (Figure 7A). Notably, B/B treatment impacted a much smaller set of transcripts in the presence of KN93 compared with inhibitormatched control cultures (1,953 DEGs), suggesting that a large proportion of the RIPK3-dependent transcriptional response was dependent on CaMKII function (Figure 7B). Inhibition of CREB using 666-15 had a comparatively smaller impact compared with blockade of CaMKII but nevertheless substantially decreased the number of significant DEGs induced by B/B (4,572 DEGs) (Figure 7C). These data suggest that CREB is likely only one of potentially many targets of CaMKII activity downstream of RIPK3 activation in neurons. However, given our functional data demonstrating a requirement for CREB in RIPK3-mediated neuroprotection, we sought to further characterize the CREB-dependent portion of the transcriptomic shift induced by B/B. IPA revealed that B/B treatment altered several pathways with relevance to our study, including terms related to Ca²⁺ influx and abundance, as well as epilepsy and neurotransmitter quantity (Figure 7D). By contrast, these transcriptional shifts were notably blunted in the setting of either CaMKII or CREB inhibition and, indeed, RIPK3 activation even activated rather than suppressed genes associated with Ca²⁺ mobilization

in the presence of either inhibitor. Further analysis of additional gene modules relevant to our functional studies revealed that RIPK3 activation suppressed representative genes whose expression is induced in an activity-dependent manner (Figure 7E), as well as genes related to glutamate receptor signaling (Figure 7F), and epilepsy/seizures (Figure 7G). By contrast, expression within these gene modules was markedly higher in the presence of KN93, while 666-15 treatment resulted in intermediate expression that was nevertheless higher than that observed in cultures treated with B/B and no inhibitor. A converse phenotype was observed in gene modules related to the suppression of cell death (Figure 7H) and neuroprotection (Figure 7I), which were strongly upregulated by B/B alone but were less so when either CaMKII or CREB was inhibited. Notably, expression of the top DEGs associated with inflammatory signaling in our analysis was not impacted by either CaMKII or CREB inhibition (Figure S7A), suggesting that the CaMKII/ CREB-mediated arm of RIPK3 signaling is not directly involved in the traditional inflammatory outputs of this pathway. These patterns of expression are all consistent with the idea that RIPK3 activation suppresses genes associated with neuronal excitation and supports expression of genes associated with neuroprotection, in a strongly CaMKII-dependent manner and at least partially in a CREB-dependent manner.

Given these results, we performed additional pathogenesis studies to confirm that RIPK3-mediated neuroprotection was dependent on CREB in vivo. Ripk3-2xFVf1/f1 Syn1 Cre+ mice were infected with ZIKV, followed by intracerebroventricular (i.c.v.) administration of B/B simultaneously with a CaMKII inhibitor (AIP) or CREB inhibitor (666-15) on day 3 post infection (Figure 7J). Chemogenetic activation of neuronal RIPK3 conferred significant protection from ZIKV infection, as B/B treatment resulted in enhanced survival and diminished clinical disease following infection in Ripk3-2xFV^{fl/fl} Syn1 Cre+ mice (Figures 7K and S7B) but not in Cre- littermate controls (Figure S7C). Cotreatment with inhibitors of either CaMKII or CREB abrogated the protective effects of enforced RIPK3 activation in neurons. Notably, we did not detect differences in CNS viral burden due to these treatments, suggesting that CaMKII and CREB do not exert neuroprotection through direct suppression of viral replication (Figure S7D). Together, these results suggest that the CaMKII- and CREB-dependent outputs of RIPK3-mediated transcriptional activation are required to promote host survival during flavivirus encephalitis.

DISCUSSION

Recent work has uncovered complex and nuanced roles for immune signaling in the modulation of neural activity. For example, social behavior has been shown to invoke JAK/STAT-mediated transcription that controls neural activity, suggesting evolutionary links between canonical immune and neurologic signaling pathways.⁵² More recently, the molecular basis of memory formation has also been shown to involve innate immune sensing of

(H–J) MultiTox cell viability assay in Ripk3-2xFV^{fl/fl} Nestin Cre⁺ neurons treated with B/B homodimerizer for 24 h with or without indicated inhibitors of CREB (H), de novo transcription (I), or de novo translation (J), followed by exposure to NMDA. Panels report live (AFC) and dead (R110) protease activity. n = 6 independent cultures per group/condition pooled from 2 independent experiments. *p < 0.5, **p < 0.01, ***p < 0.001. Error bars represent SEM.



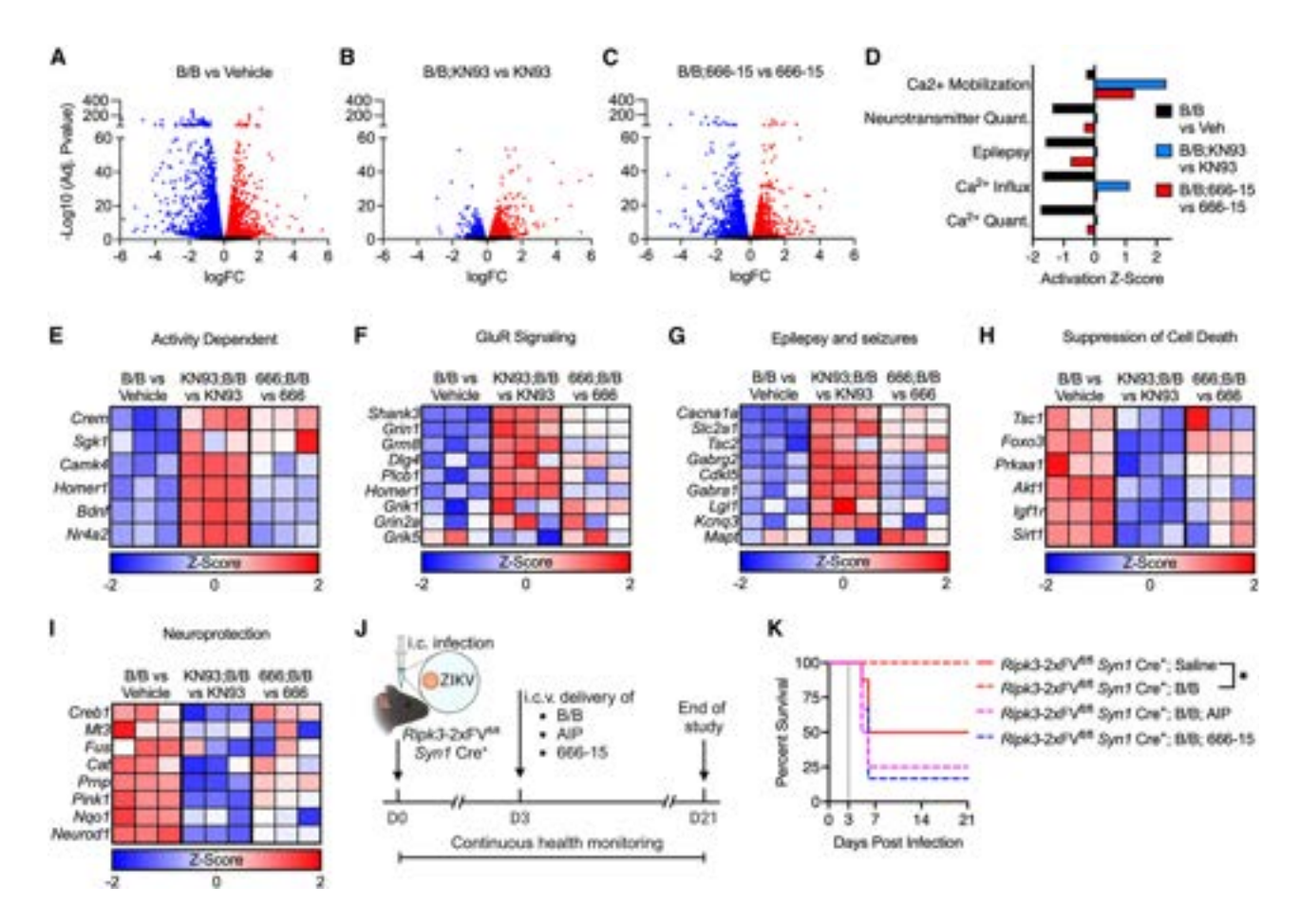


Figure 7. RIPK3 activation induces a CaMKII- and CREB-dependent neuroprotective transcriptional program

(A–I) Ripk3-2xFV^{II/II} Nestin Cre⁺ cortical neuron cultures were treated with indicated drugs for 24 h and then subjected to bulk RNA sequencing. n = 3 independent cultures per group/condition. (A-C) Volcano plots showing significant DEGs. Data points in red exhibit upregulated expression, while those in blue exhibit downregulated expression. Genes with FDR < 0.05 were considered significant. (D) Selected significantly enriched IPA terms showing activation scores within each of the indicated comparisons. (E-I) Heatmaps showing selected significant DEGs associated with indicated pathways. Data are expressed as Z scores of log₂-fold change values within each comparison.

(J) Schematic showing treatment paradigm in which Ripk3-2xFV^{fl/fl} Syn1 Cre+ mice were intracranially infected with ZIKV. On day 3 post infection, mice received i.c.v. injection of indicated drugs.

(K) Survival analysis of mice in indicated treatment groups. n = 5–8 animals/group pooled from 2 independent experiments.*p < 0.05. See also Figure S7.

endogenous genomic damage induced by neural activity. 53 In the context of disease, pathogen sensors and inflammatory cytokines have been implicated in a variety of neurologic and behavioral outcomes, 54-58 including sickness behavior, 59-61 and inflammation generally is known to drive pathologic processes in neurons, including aberrant synaptic pruning, 6,62,63 excitotoxicity, 23,64,65 and epileptogenesis. 66,67 Our results describe a nexus of neuroimmune signaling in which activation of RIPK3 dampens neuronal excitability, which in turn promotes survival in the presence of excitotoxic concentrations of glutamate during CNS viral infection. These results add an additional dimension to the idea of neuroimmune control of neurotransmission by demonstrating a physiological role for this process in host protection and the suppression of viral neuropathogenesis.

Our work also adds valuable insight to our understanding of innate immunity in neurons, whose unique and vital roles in organismal health necessitate tight regulation of cell fate and survival. Extensive previous work has shown that neurons are resistant to programmed cell death⁶⁸ and that the cell-death-independent functions of RIPK3 promote control of CNS viral infection by driving immunological gene expression.^{13–15} Here, we define a more extensive role for RIPK3 in controlling neuronal biology, including unexpected functions in regulating excitatory neurotransmission. The potential for the pleiotropic kinase CaMKII⁶⁹⁻⁷¹ to be a direct substrate of RIPK3 in neurons (and other cell types) suggests a host of additional roles for RIPK3 and related proteins in regulating aspects of cell biology that extend beyond canonical immune and/or cell death processes. Whether these putative non-canonical functions of RIPK3 represent a specific evolutionary adaptation of this pathway in neurons is unknown, and an alternative hypothesis is that regulation of cell biology via transcriptional control represents the more evolutionarily ancient function of this protein that has, perhaps, been obscured by the later development of RIPK3-driven cell





death in the necroptosis-susceptible cell types in which this pathway has been traditionally studied.

In either case, the exact mechanisms that protect neurons from necroptosis during RIPK3 activation remain to be discovered. Notably, recent work has shown that overexpression of MLKL in cortical neurons does not render them susceptible to necroptosis, 72 suggesting the existence of particularly strong regulators that restrain MLKL-driven cell death in neurons. Others have noted potential mechanisms that may underlie neuronal resistance to necroptosis, such as endosomal sorting complexes required for transport-III (ESCRT-III)-mediated exocytosis of MLKL and membrane repair. 72,73 Our results showing strong engagement of CREB following RIPK3 activation provide an additional possibility, especially given the well-established roles for CREB target genes in preserving neuronal viability across a broad variety of insults. 49,74-76 Notably, CREB is known to suppress apoptosis through several mechanisms, such as upregulation of pro-survival B-cell lymphoma 2 (BCL-2) family proteins, 77,78 and thus may actively suppress necroptosis through transcriptional control of programmed cell death regulatory proteins. CREB has also been shown to suppress the transcriptional activity of NF-κB, 79,80 which itself is intricately linked with both RIPK signaling and cell survival, and thus this connection may also provide clues concerning the unique properties of RIPK3 signaling in cell types such as neurons in which CREB is highly active.

Finally, our findings also provide insight into the central role of aberrant neural excitation in the pathogenesis of viral encephalitis. While RIPK3 signaling appears to represent an endogenous mechanism of neuroprotection during flavivirus-induced neurotoxicity, this phenomenon supports the idea that pharmacologic interventions that suppress glutamatergic neurotransmission and/or engage CREB-dependent neuroprotection may have therapeutic potential during neuroinvasive flavivirus infection, particularly during acute encephalitis.²³ The role of hyperexcitation in neuronal cell death during these infections also raises the possibility that non-pharmacologic strategies such as neuromodulation81,82 may have some benefit, though testing this hypothesis will require extensive mechanistic study. In any case, identifying strategies to preserve CNS health during flavivirus infections is of critical importance given the significant and growing burden flaviviruses pose to global public health. Flaviviruses, including WNV and ZIKV, continue to circulate on multiple continents and are likely to continue causing recurrent epidemics in coming years. 83,84 Moreover, climate change continues to increase the endemic range of the mosquito vectors that transmit several medically significant flaviviruses to areas where they are not currently present.85 As numerous other emerging flaviviruses are both neurovirulent and possess epidemic potential,³¹ continued work aimed toward understanding mechanisms of neuropathogenesis and neuroprotection during flavivirus infection is especially urgent.

Limitations of the study

Ongoing work will be needed to address some limitations of this study. For example, known structural differences between mouse and human RIPK386 raise the possibility that human RIPK3 may interact with CaMKII or other neurotransmissionrelated effectors in ways not fully captured by our current

system. Moreover, although our results indicate that RIPK3 promotes CaMKII activation, we cannot exclude the possibility that CaMKII is recruited as part of a larger protein complex (such as the necrosome⁸⁷) rather than serving as a direct substrate for RIPK3. Distinguishing these scenarios will require additional biochemical and structural studies (e.g., co-immunoprecipitation, in vitro kinase assays, or advanced imaging techniques) to clarify the precise mechanistic interactions between these molecules. Finally, while our data suggest a role for RIPK3 in directly modulating neuronal activity, more direct measures of neurotransmission, including in vivo electrophysiological recordings, would provide more definitive evidence of this effect. Such experiments are technically challenging to perform under the biocontainment required when working with flaviviruses. However, overcoming such limitations will be required to study the impact of CNS infection on neuronal activity with maximum rigor in the future.

RESOURCE AVAILABILITY

Lead contact

Requests for further information and resources should be directed to and will be fulfilled by the lead contact, Brian Daniels (b.daniels@rutgers.edu).

Materials availability

This study did not generate new or unique reagents. Requests for assistance with sourcing any of the materials used in this study can be directed to the lead

Data and code availability

- RNA sequencing data have been deposited to the NCBI Gene Expression Omnibus (GEO) database under GEO: GSE264436.
- This paper does not report original code.
- Any additional information required to reanalyze the data reported in this paper is available from the lead contact upon request.

ACKNOWLEDGMENTS

This work was supported by R21 NS130282 (to B.P.D. and B.L.F.) and R01 NS120895-S2 (to B.P.D. and I.E.). I.E. was supported by an HHMI Gilliam Fellowship.

AUTHOR CONTRIBUTIONS

Conceptualization: I.E., B.L.F., and B.P.D.; investigation: I.E., B.D.B., N.P., M.L., T.-W.C., M.M., B.J.V., C.A., and B.P.D.; analysis: I.E., B.D.B., N.P., T.-W.C., M.M., B.J.V., and B.P.D.; resources: B.L.F. and B.P.D.; writing - original draft: I.E. and B.P.D.; writing - review and editing: I.E., B.J.V., B.L.F., and B.P.D.; supervision: C.A., B.L.F., and B.P.D.; funding acquisition: B.L.F. and B.P.D.

DECLARATION OF INTERESTS

The authors declare no competing interests.

STAR*METHODS

Detailed methods are provided in the online version of this paper and include the following:

- KEY RESOURCES TABLE
- EXPERIMENTAL MODELS AND STUDY PARTICIPANT DETAILS
 - Mouse lines
 - Viruses and virologic assays
 - o Cell culture and infection



- METHOD DETAILS
 - Transcriptomic analysis
 - Mouse infections and tissue harvesting
 - Cell Death Assavs
 - o Diseases & Functions, Canonical Pathways, and Kinase Regulator
 - Fluorescent In Situ Hybridization (FISH)
 - o Calcium Flux Assay
 - o siRNA Transfection
 - o Chemical reagents
 - Quantitative real-time PCR
 - o Immunofluorescence
 - o Microelectrode array (MEA) recordings
 - MEA signal processing and analysis
 - Seizure Assay
 - o FLAG Pulldown and Western Blot
- QUANTIFICATION AND STATISTICAL ANALYSIS

SUPPLEMENTAL INFORMATION

Supplemental information can be found online at https://doi.org/10.1016/j. immuni.2025.01.017.

Received: May 13, 2024 Revised: October 17, 2024 Accepted: January 30, 2025 Published: February 24, 2025

REFERENCES

- 1. Monet, M.C., and Quan, N. (2023). Complex Neuroimmune Involvement in Neurodevelopment: A Mini-Review. J. Inflamm. Res. 16, 2979-2991. https://doi.org/10.2147/JIR.S410562.
- 2. Huh, J.R., and Veiga-Fernandes, H. (2020). Neuroimmune circuits in inter-organ communication. Nat. Rev. Immunol. 20, 217-228. https://doi. org/10.1038/s41577-019-0247-z.
- 3. Ratsika, A., Cruz Pereira, J.S., Lynch, C.M.K., Clarke, G., and Cryan, J.F. (2023). Microbiota-immune-brain interactions: A lifespan perspective. Curr. Opin. Neurobiol. 78, 102652. https://doi.org/10.1016/j.conb.2022.
- 4. Zengeler, K.E., and Lukens, J.R. (2021). Innate immunity at the crossroads of healthy brain maturation and neurodevelopmental disorders. Nat. Rev. Immunol. 21, 454-468. https://doi.org/10.1038/s41577-020-00487-7
- 5. Salvador, A.F., de Lima, K.A., and Kipnis, J. (2021). Neuromodulation by the immune system: a focus on cytokines. Nat. Rev. Immunol. 21, 526-541. https://doi.org/10.1038/s41577-021-00508-z.
- 6. Zipp, F., Bittner, S., and Schafer, D.P. (2023). Cytokines as emerging regulators of central nervous system synapses. Immunity 56, 914-925. https://doi.org/10.1016/j.immuni.2023.04.011.
- 7. Villasana-Salazar, B., and Vezzani, A. (2023). Neuroinflammation microenvironment sharpens seizure circuit. Neurobiol. Dis. 178, 106027. https://doi.org/10.1016/j.nbd.2023.106027.
- 8. Johnson, K.V.A., and Foster, K.R. (2018). Why does the microbiome affect behaviour? Nat. Rev. Microbiol. 16, 647-655. https://doi.org/10. 1038/s41579-018-0014-3.
- 9. Koo, J.W., and Wohleb, E.S. (2021). How Stress Shapes Neuroimmune Function: Implications for the Neurobiology of Psychiatric Disorders. Biol. Psychiatry 90, 74-84. https://doi.org/10.1016/j.biopsych.2020.
- 10. Angel, J.P., and Daniels, B.P. (2022). Paradoxical roles for programmed cell death signaling during viral infection of the central nervous system. Curr. Opin. Neurobiol. 77, 102629. https://doi.org/10.1016/j.conb.2022.
- 11. Wu, L., Chung, J.Y., Cao, T., Jin, G., Edmiston, W.J., 3rd, Hickman, S., Levy, E.S., Whalen, J.A., Abrams, E.S.L., Degterev, A., et al. (2021).

- Genetic inhibition of RIPK3 ameliorates functional outcome in controlled cortical impact independent of necroptosis. Cell Death Dis. 12, 1064. https://doi.org/10.1038/s41419-021-04333-z.
- 12. Guo, H., Koehler, H.S., Mocarski, E.S., and Dix, R.D. (2022). RIPK3 and caspase 8 collaborate to limit herpes simplex encephalitis. PLoS Pathog. 18, e1010857. https://doi.org/10.1371/journal.ppat.1010857.
- 13. Daniels, B.P., Kofman, S.B., Smith, J.R., Norris, G.T., Snyder, A.G., Kolb, J.P., Gao, X., Locasale, J.W., Martinez, J., Gale, M., Jr., et al. (2019). The Nucleotide Sensor ZBP1 and Kinase RIPK3 Induce the Enzyme IRG1 to Promote an Antiviral Metabolic State in Neurons. Immunity 50, 64-76.e4. https://doi.org/10.1016/j.immuni.2018.11.017.
- 14. Daniels, B.P., Snyder, A.G., Olsen, T.M., Orozco, S., Oguin, T.H., 3rd, Tait, S.W.G., Martinez, J., Gale, M., Jr., Loo, Y.M., and Oberst, A. (2017). RIPK3 Restricts Viral Pathogenesis via Cell Death-Independent Neuroinflammation. Cell 169, 301-313.e11. https://doi.org/10.1016/j. cell.2017.03.011.
- 15. Lindman, M., Angel, J.P., Estevez, I., Chang, N.P., Chou, T.W., McCourt, M., Atkins, C., and Daniels, B.P. (2023). RIPK3 promotes brain regionspecific interferon signaling and restriction of tick-borne flavivirus infection. PLoS Pathog. 19, e1011813. https://doi.org/10.1371/journal.ppat. 1011813.
- 16. Sah, E., Krishnamurthy, S., Ahmidouch, M.Y., Gillispie, G.J., Milligan, C., and Orr, M.E. (2021). The Cellular Senescence Stress Response in Post-Mitotic Brain Cells: Cell Survival at the Expense of Tissue Degeneration. Life (Basel) 11, 229. https://doi.org/10.3390/life11030229.
- 17. Daniels, B.P., and Oberst, A. (2023). Outcomes of RIP Kinase Signaling During Neuroinvasive Viral Infection. Curr. Top. Microbiol. Immunol. 442, 155-174. https://doi.org/10.1007/82_2020_204.
- 18. Löscher, W., and Howe, C.L. (2022). Molecular Mechanisms in the Genesis of Seizures and Epilepsy Associated With Viral Infection. Front. Mol. Neurosci. 15, 870868. https://doi.org/10.3389/fnmol.2022.
- 19. Gorska, A.M., and Eugenin, E.A. (2020). The Glutamate System as a Crucial Regulator of CNS Toxicity and Survival of HIV Reservoirs. Front. Cell. Infect. Microbiol. 10, 261. https://doi.org/10.3389/fcimb.
- 20. Darman, J., Backovic, S., Dike, S., Maragakis, N.J., Krishnan, C., Rothstein, J.D., Irani, D.N., and Kerr, D.A. (2004), Viral-induced spinal motor neuron death is non-cell-autonomous and involves glutamate excitotoxicity. J. Neurosci. 24, 7566-7575. https://doi.org/10.1523/ JNEUROSCI.2002-04.2004.
- 21. Nargi-Aizenman, J.L., Havert, M.B., Zhang, M., Irani, D.N., Rothstein, J.D., and Griffin, D.E. (2004). Glutamate receptor antagonists protect from virus-induced neural degeneration. Ann. Neurol. 55, 541-549. https://doi.org/10.1002/ana.20033.
- 22. Brison, E., Jacomy, H., Desforges, M., and Talbot, P.J. (2011). Glutamate excitotoxicity is involved in the induction of paralysis in mice after infection by a human coronavirus with a single point mutation in its spike protein. J. Virol. 85, 12464-12473. https://doi.org/10.1128/JVI.05576-11.
- 23. Nogueira, C.O., Rocha, T., Messor, D.F., Souza, I.N.O., and Clarke, J.R. (2023). Fundamental neurochemistry review: Glutamatergic dysfunction as a central mechanism underlying flavivirus-induced neurological damage. J. Neurochem. 166, 915-927. https://doi.org/10.1111/jnc.15935.
- 24. Gaburro, J., Bhatti, A., Sundaramoorthy, V., Dearnley, M., Green, D., Nahavandi, S., Paradkar, P.N., and Duchemin, J.B. (2018). Zika virusinduced hyper excitation precedes death of mouse primary neuron. Virol. J. 15, 79. https://doi.org/10.1186/s12985-018-0989-4.
- 25. Blakely, P.K., Kleinschmidt-DeMasters, B.K., Tyler, K.L., and Irani, D.N. (2009). Disrupted glutamate transporter expression in the spinal cord with acute flaccid paralysis caused by West Nile virus infection. J. Neuropathol. Exp. Neurol. 68, 1061-1072. https://doi.org/10.1097/ NEN.0b013e3181b8ba14.
- 26. Costa, V.V., Del Sarto, J.L., Rocha, R.F., Silva, F.R., Doria, J.G., Olmo, I.G., Marques, R.E., Queiroz-Junior, C.M., Foureaux, G., Araújo, J.M.S., et al. (2017). N-Methyl-d-Aspartate (NMDA) Receptor Blockade





- Prevents Neuronal Death Induced by Zika Virus Infection. mBio 8, e0035017. https://doi.org/10.1128/mBio.00350-17.
- Zhou, X., Hollern, D., Liao, J., Andrechek, E., and Wang, H. (2013). NMDA receptor-mediated excitotoxicity depends on the coactivation of synaptic and extrasynaptic receptors. Cell Death Dis. 4, e560. https://doi.org/ 10.1038/cddis.2013.82.
- Vezzani, A., and Viviani, B. (2015). Neuromodulatory properties of inflammatory cytokines and their impact on neuronal excitability. Neuropharmacology 96, 70–82. https://doi.org/10.1016/j.neuropharm.2014.10.027.
- Iori, V., Frigerio, F., and Vezzani, A. (2016). Modulation of neuronal excitability by immune mediators in epilepsy. Curr. Opin. Pharmacol. 26, 118–123. https://doi.org/10.1016/j.coph.2015.11.002.
- Bifani, A.M., Chan, K.W.K., Borrenberghs, D., Tan, M.J.A., Phoo, W.W., Watanabe, S., Goethals, O., Vasudevan, S.G., and Choy, M.M. (2023). Therapeutics for flaviviral infections. Antiviral Res. 210, 105517. https://doi.org/10.1016/j.antiviral.2022.105517.
- Pierson, T.C., and Diamond, M.S. (2020). The continued threat of emerging flaviviruses. Nat. Microbiol. 5, 796–812. https://doi.org/10. 1038/s41564-020-0714-0
- Olmo, I.G., Carvalho, T.G., Costa, V.V., Alves-Silva, J., Ferrari, C.Z., Izidoro-Toledo, T.C., Da Silva, J.F., Teixeira, A.L., Souza, D.G., Marques, J.T., et al. (2017). Zika Virus Promotes Neuronal Cell Death in a Non-Cell Autonomous Manner by Triggering the Release of Neurotoxic Factors. Front. Immunol. 8, 1016. https://doi.org/10.3389/ fimmu.2017.01016.
- Chen, C.-J., Ou, Y.-C., Chang, C.-Y., Pan, H.-C., Liao, S.-L., Chen, S.-Y., Raung, S.-L., and Lai, C.-Y. (2012/03/01). Glutamate released by Japanese encephalitis virus-infected microglia involves TNF-α signaling and contributes to neuronal death. Glia 60, 487–501. https://doi.org/10. 1002/glia.22282.
- Nayak, P.K., and Kerr, D.S. (2013/03/01). Low-dose GYKI-52466: Prophylactic preconditioning confers long-term neuroprotection and functional recovery following hypoxic-ischaemic brain injury. Neuroscience 232, 128–138. https://doi.org/10.1016/j.neuroscience. 2012.11.063.
- Newton, K., Dugger, D.L., Maltzman, A., Greve, J.M., Hedehus, M., Martin-McNulty, B., Carano, R.A., Cao, T.C., van Bruggen, N., Bernstein, L., et al. (2016). RIPK3 deficiency or catalytically inactive RIPK1 provides greater benefit than MLKL deficiency in mouse models of inflammation and tissue injury. Cell Death Differ. 23, 1565–1576. https://doi.org/10.1038/cdd.2016.46.
- Zhu, Y., Romero, M.I., Ghosh, P., Ye, Z., Charnay, P., Rushing, E.J., Marth, J.D., and Parada, L.F. (2001). Ablation of NF1 function in neurons induces abnormal development of cerebral cortex and reactive gliosis in the brain. Genes Dev. 15, 859–876. https://doi.org/10.1101/gad.862101.
- Svalbe, B., Stelfa, G., Vavers, E., Zvejniece, B., Grinberga, S., Sevostjanovs, E., Pugovics, O., Dambrova, M., and Zvejniece, L. (2019/10/17). Effects of the N-methyl-d-aspartate receptor antagonist, MK-801, on spatial memory and influence of the route of administration. Behav. Brain Res. 372, 112067. https://doi.org/10.1016/j.bbr.2019.
- Niles, A.L., Moravec, R.A., and Riss, T.L. (2009). In vitro viability and cytotoxicity testing and same-well multi-parametric combinations for high throughput screening. Curr. Chem. Genomics 3, 33–41. https://doi.org/ 10.2174/1875397300903010033.
- Choi, D.W. (1988/01/01). Calcium-mediated neurotoxicity: relationship to specific channel types and role in ischemic damage. Trends Neurosci. 11, 465–469. https://doi.org/10.1016/0166-2236(88)90200-7.
- Ankarcrona, M., Dypbukt, J.M., Bonfoco, E., Zhivotovsky, B., Orrenius, S., Lipton, S.A., and Nicotera, P. (1995). Glutamate-induced neuronal death: A succession of necrosis or apoptosis depending on mitochondrial function. Neuron 15, 961–973. https://doi.org/10.1016/0896-6273.
- Choi, D.W. (1988/10/01). Glutamate neurotoxicity and diseases of the nervous system. Neuron 1, 623–634. https://doi.org/10.1016/0896-6273(88)90162-6.

- Snyder, A.G., Hubbard, N.W., Messmer, M.N., Kofman, S.B., Hagan, C.E., Orozco, S.L., Chiang, K., Daniels, B.P., Baker, D., and Oberst, A. (2019). Intratumoral activation of the necroptotic pathway components RIPK1 and RIPK3 potentiates antitumor immunity. Sci. Immunol. 4, eaaw2004. https://doi.org/10.1126/sciimmunol.aaw2004.
- Krämer, A., Green, J., Pollard, J., and Tugendreich, S. (02/15/2014).
 Causal analysis approaches in Ingenuity Pathway Analysis.
 Bioinformatics Oxf. Engl. 30, 523–530. https://doi.org/10.1093/bioinformatics/btt703.
- Soto-Otero, R., Mendez-Alvarez, E., Sierra-Paredes, G., Galan-Valiente, J., Aguilar-Veiga, E., and Sierra-Marcuño, G. (1987/09/01). High-performance liquid chromatographic procedure for quantitative determination of pentylenetetrazol in serum and discrete areas of rat brain. Anal. Biochem. 165, 331–336. https://doi.org/10.1016/0003-2697(87)90277-6.
- Van Erum, J., Van Dam, D., and De Deyn, P.P. (2019). PTZ-induced seizures in mice require a revised Racine scale. Epilepsy Behav. 95, 51–55. https://doi.org/10.1016/j.yebeh.2019.02.029.
- Ashpole, N.M., Song, W., Brustovetsky, T., Engleman, E.A., Brustovetsky, N., Cummins, T.R., and Hudmon, A. (2012). Calcium/ calmodulin-dependent protein kinase II (CaMKII) inhibition induces neurotoxicity via dysregulation of glutamate/calcium signaling and hyperexcitability. J. Biol. Chem. 287, 8495–8506. https://doi.org/10.1074/ ibc.M111.323915.
- Guo, X., Zhou, J., Starr, C., Mohns, E.J., Li, Y., Chen, E.P., Yoon, Y., Kellner, C.P., Tanaka, K., Wang, H., et al. (2021). Preservation of vision after CaMKII-mediated protection of retinal ganglion cells. Cell 184, 4299–4314.e12. https://doi.org/10.1016/j.cell.2021.06.031.
- Zhang, T., Zhang, Y., Cui, M., Jin, L., Wang, Y., Lv, F., Liu, Y., Zheng, W., Shang, H., Zhang, J., et al. (2016). CaMKII is a RIP3 substrate mediating ischemia- and oxidative stress-induced myocardial necroptosis. Nat. Med. 22, 175–182. https://doi.org/10.1038/nm.4017.
- Sakamoto, K., Karelina, K., and Obrietan, K. (2011). CREB: a multifaceted regulator of neuronal plasticity and protection. J. Neurochem. 116, 1–9. https://doi.org/10.1111/j.1471-4159.2010.07080.x.
- Walton, M.R., and Dragunow, I. (2000). Is CREB a key to neuronal survival? Trends Neurosci. 23, 48–53. https://doi.org/10.1016/s0166-2236(99)01500-3.
- Hardingham, G.E., Fukunaga, Y., and Bading, H. (2002). Extrasynaptic NMDARs oppose synaptic NMDARs by triggering CREB shut-off and cell death pathways. Nat. Neurosci. 5, 405–414. https://doi.org/10. 1038/nn835.
- Filiano, A.J., Xu, Y., Tustison, N.J., Marsh, R.L., Baker, W., Smirnov, I., Overall, C.C., Gadani, S.P., Turner, S.D., Weng, Z., et al. (2016). Unexpected role of interferon-gamma in regulating neuronal connectivity and social behaviour. Nature 535, 425–429. https://doi.org/10.1038/ nature18626.
- Jovasevic, V., Wood, E.M., Cicvaric, A., Zhang, H., Petrovic, Z., Carboncino, A., Parker, K.K., Bassett, T.E., Moltesen, M., Yamawaki, N., et al. (2024). Formation of memory assemblies through the DNAsensing TLR9 pathway. Nature 628, 145–153. https://doi.org/10.1038/ s41586-024-07220-7.
- Yang, L., Huh, J.R., and Choi, G.B. (2023). One messenger shared by two systems: How cytokines directly modulate neurons. Curr. Opin. Neurobiol. 80, 102708. https://doi.org/10.1016/j.conb.2023.102708.
- 55. Yao, H., Zhang, D., Yu, H., Yuan, H., Shen, H., Lan, X., Liu, H., Chen, X., Meng, F., Wu, X., et al. (2023). Gut microbiota regulates chronic ethanol exposure-induced depressive-like behavior through hippocampal NLRP3-mediated neuroinflammation. Mol. Psychiatry 28, 919–930. https://doi.org/10.1038/s41380-022-01841-y.
- Sha, Q., Madaj, Z., Keaton, S., Escobar Galvis, M.L., Smart, L., Krzyzanowski, S., Fazleabas, A.T., Leach, R., Postolache, T.T., Achtyes, E.D., and Brundin, L. (2022). Cytokines and tryptophan metabolites can predict depressive symptoms in pregnancy. Transl. Psychiatry 12, 35. https://doi.org/10.1038/s41398-022-01801-8.



- Hughes, H.K., Moreno, R.J., and Ashwood, P. (2023). Innate immune dysfunction and neuroinflammation in autism spectrum disorder (ASD). Brain Behav. Immun. 108, 245–254. https://doi.org/10.1016/j.bbi.2022. 12.001.
- Pagoni, P., Korologou-Linden, R.S., Howe, L.D., Davey Smith, G., Ben-Shlomo, Y., Stergiakouli, E., and Anderson, E.L. (2022). Causal effects of circulating cytokine concentrations on risk of Alzheimer's disease and cognitive function. Brain Behav. Immun. 104, 54–64. https://doi.org/10.1016/j.bbi.2022.05.006.
- Kurki, S.N., Ala-Kurikka, T., Lipponen, A., Pospelov, A.S., Rolova, T., Koistinaho, J., Voipio, J., and Kaila, K. (2023). A brain cytokine-independent switch in cortical activity marks the onset of sickness behavior triggered by acute peripheral inflammation. J. Neuroinflammation 20, 176. https://doi.org/10.1186/s12974-023-02851-5.
- Turkheimer, F.E., Veronese, M., Mondelli, V., Cash, D., and Pariante, C.M. (2023). Sickness behaviour and depression: An updated model of peripheral-central immunity interactions. Brain Behav. Immun. 111, 202–210. https://doi.org/10.1016/j.bbi.2023.03.031.
- Devlin, B.A., Smith, C.J., and Bilbo, S.D. (2022). Sickness and the Social Brain: How the Immune System Regulates Behavior across Species. Brain Behav. Evol. 97, 197–210. https://doi.org/10.1159/000521476.
- Vasek, M.J., Garber, C., Dorsey, D., Durrant, D.M., Bollman, B., Soung, A., Yu, J., Perez-Torres, C., Frouin, A., Wilton, D.K., et al. (2016). A complement-microglial axis drives synapse loss during virus-induced memory impairment. Nature 534, 538–543. https://doi.org/10.1038/ nature18283.
- 63. Wang, J., Chen, H.S., Li, H.H., Wang, H.J., Zou, R.S., Lu, X.J., Wang, J., Nie, B.B., Wu, J.F., Li, S., et al. (2023). Microglia-dependent excessive synaptic pruning leads to cortical underconnectivity and behavioral abnormality following chronic social defeat stress in mice. Brain Behav. Immun. 109, 23–36. https://doi.org/10.1016/j.bbi.2022.12.019.
- 64. Viviani, B., Bartesaghi, S., Gardoni, F., Vezzani, A., Behrens, M.M., Bartfai, T., Binaglia, M., Corsini, E., Di Luca, M., Galli, C.L., et al. (2003). Interleukin-1beta enhances NMDA receptor-mediated intracellular calcium increase through activation of the Src family of kinases. J. Neurosci. 23, 8692–8700. https://doi.org/10.1523/JNEUROSCI.23-25-08692.2003.
- Lotz, S.K., Blackhurst, B.M., Reagin, K.L., and Funk, K.E. (2021).
 Microbial Infections Are a Risk Factor for Neurodegenerative Diseases.
 Front. Cell. Neurosci. 15, 691136. https://doi.org/10.3389/fncel.2021.
 691136.
- Soltani Khaboushan, A., Yazdanpanah, N., and Rezaei, N. (2022).
 Neuroinflammation and Proinflammatory Cytokines in Epileptogenesis.
 Mol. Neurobiol. 59, 1724–1743. https://doi.org/10.1007/s12035-022-02725-6
- Chen, Y., Nagib, M.M., Yasmen, N., Sluter, M.N., Littlejohn, T.L., Yu, Y., and Jiang, J. (2023). Neuroinflammatory mediators in acquired epilepsy: an update. Inflamm. Res. 72, 683–701. https://doi.org/10.1007/s00011-023-01700-8.
- Hollville, E., Romero, S.E., and Deshmukh, M. (2019). Apoptotic cell death regulation in neurons. FEBS Journal 286, 3276–3298. https://doi. org/10.1111/febs.14970.
- Wang, Q., Hernández-Ochoa, E.O., Viswanathan, M.C., Blum, I.D., Do, D.C., Granger, J.M., Murphy, K.R., Wei, A.C., Aja, S., Liu, N., et al. (2021). CaMKII oxidation is a critical performance/disease trade-off acquired at the dawn of vertebrate evolution. Nat. Commun. 12, 3175. https://doi.org/10.1038/s41467-021-23549-3.
- Jiang, S.J., and Wang, W. (2020). Research progress on the role of CaMKII in heart disease. Am. J. Transl. Res. 12, 7625–7639.
- Yasuda, R., Hayashi, Y., and Hell, J.W. (2022). CaMKII: a central molecular organizer of synaptic plasticity, learning and memory. Nat. Rev. Neurosci. 23, 666–682. https://doi.org/10.1038/s41583-022-00624-2.
- Kofman, S.B., Chu, L.H., Ames, J.M., Chavarria, S.D., Lichauco, K., Daniels, B.P., and Oberst, A. (2024). RIPK3 coordinates RHIM domain-

- dependent inflammatory transcription in neurons. Preprint at bioRxiv. https://doi.org/10.1101/2024.02.29.582857.
- Gong, Y.N., Guy, C., Olauson, H., Becker, J.U., Yang, M., Fitzgerald, P., Linkermann, A., and Green, D.R. (2017). ESCRT-III Acts Downstream of MLKL to Regulate Necroptotic Cell Death and Its Consequences. Cell 169, 286–300.e16. https://doi.org/10.1016/j.cell.2017.03.020.
- Sharma, V.K., and Singh, T.G. (2020). CREB: A Multifaceted Target for Alzheimer's Disease. Curr. Alzheimer Res. 17, 1280–1293. https://doi. org/10.2174/1567205018666210218152253.
- Khan, H., Bangar, A., Grewal, A.K., and Singh, T.G. (2023). Mechanistic Implications of GSK and CREB Crosstalk in Ischemia Injury. Neurotox. Res. 42, 1. https://doi.org/10.1007/s12640-023-00680-1.
- Chowdhury, M.A.R., An, J., and Jeong, S. (2023). The Pleiotropic Face of CREB Family Transcription Factors. Mol. Cells 46, 399–413. https://doi. org/10.14348/molcells.2023.2193.
- Wilson, B.E., Mochon, E., and Boxer, L.M. (1996). Induction of bcl-2 expression by phosphorylated CREB proteins during B-cell activation and rescue from apoptosis. Mol. Cell. Biol. 16, 5546–5556. https://doi.org/10.1128/MCB.16.10.5546.
- Pugazhenthi, S., Nesterova, A., Sable, C., Heidenreich, K.A., Boxer, L.M., Heasley, L.E., and Reusch, J.E. (2000). Akt/protein kinase B up-regulates Bcl-2 expression through cAMP-response element-binding protein.
 J. Biol. Chem. 275, 10761–10766. https://doi.org/10.1074/jbc.275. 15.10761.
- Zhong, H., Voll, R.E., and Ghosh, S. (1998). Phosphorylation of NF-kappa B p65 by PKA stimulates transcriptional activity by promoting a novel bivalent interaction with the coactivator CBP/p300. Mol. Cell 1, 661–671. https://doi.org/10.1016/s1097-2765(00)80066-0.
- Parry, G.C., and Mackman, N. (1997). Role of cyclic AMP response element-binding protein in cyclic AMP inhibition of NF-kappaB-mediated transcription. J. Immunol. 159, 5450–5456. https://doi.org/10.4049/jim-munol.159.11.5450.
- Ryvlin, P., Rheims, S., Hirsch, L.J., Sokolov, A., and Jehi, L. (2021).
 Neuromodulation in epilepsy: state-of-the-art approved therapies.
 Lancet Neurol. 20, 1038–1047. https://doi.org/10.1016/S1474-4422(21) 00300-8
- Salama, H., Salama, A., Oscher, L., Jallo, G.I., and Shimony, N. (2024). The role of neuromodulation in the management of drug-resistant epilepsy. Neurol. Sci. 45, 4243–4268. https://doi.org/10.1007/s10072-024-07513-9.
- Espinal, M.A., Andrus, J.K., Jauregui, B., Waterman, S.H., Morens, D.M., Santos, J.I., Horstick, O., Francis, L.A., and Olson, D. (2019). Emerging and Reemerging Aedes-Transmitted Arbovirus Infections in the Region of the Americas: Implications for Health Policy. Am. J. Public Health 109, 387–392. https://doi.org/10.2105/AJPH.2018.304849.
- 84. Čabanová, V., Kerlik, J., Kirschner, P., Rosochová, J., Klempa, B., Sláviková, M., and Ličková, M. (2023). Co-Circulation of West Nile, Usutu, and Tick-Borne Encephalitis Viruses in the Same Area: A Great Challenge for Diagnostic and Blood and Organ Safety. Viruses 15, 366. https://doi.org/10.3390/v15020366.
- Asad, H., and Carpenter, D.O. (2018). Effects of climate change on the spread of zika virus: a public health threat. Rev. Environ. Health 33, 31–42. https://doi.org/10.1515/reveh-2017-0042.
- Meng, Y., Davies, K.A., Fitzgibbon, C., Young, S.N., Garnish, S.E., Horne, C.R., Luo, C., Garnier, J.M., Liang, L.Y., Cowan, A.D., et al. (2021).
 Human RIPK3 maintains MLKL in an inactive conformation prior to cell death by necroptosis. Nat. Commun. 12, 6783. https://doi.org/10.1038/s41467-021-27032-x.
- Li, J., McQuade, T., Siemer, A.B., Napetschnig, J., Moriwaki, K., Hsiao, Y.S., Damko, E., Moquin, D., Walz, T., McDermott, A., et al. (2012). The RIP1/RIP3 necrosome forms a functional amyloid signaling complex required for programmed necrosis. Cell 150, 339–350. https://doi.org/ 10.1016/j.cell.2012.06.019.





- 88. Newton, K., Sun, X., and Dixit, V.M. (2004). Kinase RIP3 is dispensable for normal NF-kappa Bs, signaling by the B-cell and T-cell receptors, tumor necrosis factor receptor 1, and Toll-like receptors 2 and 4. Mol. Cell. Biol. 24, 1464-1469. https://doi.org/10.1128/MCB.24.4.1464-1469.2004.
- 89. Murphy, J.M., Czabotar, P.E., Hildebrand, J.M., Lucet, I.S., Zhang, J.G., Alvarez-Diaz, S., Lewis, R., Lalaoui, N., Metcalf, D., Webb, A.I., et al. (2013). The pseudokinase MLKL mediates necroptosis via a molecular switch mechanism. Immunity 39, 443-453. https://doi.org/10.1016/j.immuni.2013.06.018.
- 90. Hubbard, N.W., Ames, J.M., Maurano, M., Chu, L.H., Somfleth, K.Y., Gokhale, N.S., Werner, M., Snyder, J.M., Lichauco, K., Savan, R., et al. (2022). ADAR1 mutation causes ZBP1-dependent immunopathology. Nature 607, 769-775. https://doi.org/10.1038/s41586-022-04896-7.
- 91. Sai, K., Parsons, C., House, J.S., Kathariou, S., and Ninomiya-Tsuji, J. (2019). Necroptosis mediators RIPK3 and MLKL suppress intracellular Listeria replication independently of host cell killing. J. Cell Biol. 218, 1994-2005. https://doi.org/10.1083/jcb.201810014.
- 92. Xie, Y., Zhao, Y., Shi, L., Li, W., Chen, K., Li, M., Chen, X., Zhang, H., Li, T., Matsuzawa-Ishimoto, Y., et al. (2020). Gut epithelial TSC1/mTOR controls RIPK3-dependent necroptosis in intestinal inflammation and cancer. J. Clin. Invest. 130, 2111-2128. https://doi.org/10.1172/JCl133264.
- 93. May, F.J., Li, L., Davis, C.T., Galbraith, S.E., and Barrett, A.D.T. (2010). Multiple pathways to the attenuation of West Nile virus in south-east Texas in 2003. Virology 405, 8-14. https://doi.org/10.1016/j.virol.2010. 04.022.
- 94. Gorman, M.J., Caine, E.A., Zaitsev, K., Begley, M.C., Weger-Lucarelli, J., Uccellini, M.B., Tripathi, S., Morrison, J., Yount, B.L., Dinnon, K.H., 3rd, et al. (2018). An immunocompetent mouse model of zika virus infection.

- Cell Host Microbe 23, 672-685.e6. https://doi.org/10.1016/j.chom.2018. 04.003
- 95. Kung, P.L., Chou, T.W., Lindman, M., Chang, N.P., Estevez, I., Buckley, B.D., Atkins, C., and Daniels, B.P. (2022). Zika virus-induced TNF-alpha signaling dysregulates expression of neurologic genes associated with psychiatric disorders. J. Neuroinflammation 19, 100. https://doi.org/10. 1186/s12974-022-02460-8.
- 96. O'Brown, N.M., Patel, N.B., Hartmann, U., Klein, A.M., Gu, C., and Megason, S.G. (2023). The secreted neuronal signal Spock1 promotes blood-brain barrier development. Dev. Cell 58, 1534-1547.e6. https:// doi.org/10.1016/j.devcel.2023.06.005.
- 97. O'Neill, K.M., Anderson, E.D., Mukherjee, S., Gandu, S., McEwan, S.A., Omelchenko, A., Rodriguez, A.R., Losert, W., Meaney, D.F., Babadi, B., and Firestein, B.L. (2023). Time-dependent homeostatic mechanisms underlie brain-derived neurotrophic factor action on neural circuitry. Commun. Biol. 6, 1278. https://doi.org/10.1038/s42003-023-05638-9.
- 98. Sullivan, D., Vaglio, B.J., Cararo-Lopes, M.M., Wong, R.D.P., Graudejus, O., and Firestein, B.L. (2024). Stretch-Induced Injury Affects Cortical Neuronal Networks in a Time- and Severity-Dependent Manner. Ann. Biomed. Eng. 52, 1021-1038. https://doi.org/10.1007/s10439-023-03438-0.
- 99. Obien, M.E.J., Deligkaris, K., Bullmann, T., Bakkum, D.J., and Frey, U. (2014). Revealing neuronal function through microelectrode array recordings. Front. Neurosci. 8, 423. https://doi.org/10.3389/fnins.2014.00423.
- 100. Rubinov, M., and Sporns, O. (2010). Complex network measures of brain connectivity: uses and interpretations. Neuroimage 52, 1059-1069. https://doi.org/10.1016/j.neuroimage.2009.10.003.



STAR***METHODS**

KEY RESOURCES TABLE

REAGENT or RESOURCE	SOURCE	IDENTIFIER
Antibodies		
Chicken anti-MAP2	Thermo Fisher Scientific	Cat# PA1-16751, RRID:AB_2138189
Chicken anti-Actin	Sigma-Aldrich	Cat# SAB3500350, RRID:AB_10638013
Chicken anti-S100b	Synaptic Systems	Cat# 287006, RRID:AB_2713986
Guinea Pig anti-NeuN	Synaptic Systems	Cat# 266004, RRID:AB_2619988
Mouse anti-CaMKIIα	Thermo Fisher Scientific	Cat# MA1-048, RRID:AB_325403
Rabbit anti-mCherry	Rockland	Cat# 600-401-P16, RRID:AB_2614470
Rabbit anti-RIPK3	Cell Signaling	Cat# 95702S, RRID:AB_2721823
Rabbit anti-Phospho CaMKIIα	Thermo Fisher Scientific	Cat# PA1-4614, RRID: AB_2259386
Rabbit anti-Phospho CREB	Thermo Fisher Scientific	Cat# MA5-11192, RRID:AB_10986840
Rat anti-GFAP	Thermo Fisher Scientific	Cat# 13-0300, RRID:AB_86543
Goat anti-rabbit 488 secondary	Thermo Fisher Scientific	Cat# A32731, RRID:AB_2633280
Goat anti-chicken 488 secondary	Thermo Fisher Scientific	Cat# A-11039, RRID: AB_2762843
Goat anti-rat 488 secondary	Thermo Fisher Scientific	Cat# A-11006, RRID:AB_141373
Goat anti-rabbit 594 secondary	Thermo Fisher Scientific	Cat# A-11012, RRID: AB_2534079
Goat anti-guinea pig 594 secondary	Thermo Fisher Scientific	Cat# A-A11076, RRID:AB_141930
Goat anti-guinea pig 647	Thermo Fisher Scientific	Cat# A21450, RRID:AB_141882
Goat anti-rabbit IRDye 800CW secondary	LicorBio	Cat# 925-32218, RRID:AB_2814922
Goat anti-mouse IRDye 800CW secondary	LicorBio	Cat# 925-32210, RRID:AB_2687825
Donkey anti-chicken IRDye 680RD secondary	LicorBio	Cat# 926-68075, RRID:AB_10974977
Bacterial and virus strains		
Zika Virus MR766 (Uganda)	WRCEVA	NR-50065
West Nile Virus Bird 114	Bobby Brooke Herrera	PMID: 20580395
Chemicals, peptides, and recombinant proteins		
Ac-YVAD	Invivogen	inh-yvad
GSK 872	GlaxoSmithKline	N/A
666-15	Sigma-Aldrich	5383410001
Actinomycin D	ThermoFisher	BP606-5
AIP	Bio-Techne	Cat #5959
AP1 (BB Homodimerizer)	Clontech	Cat# 635069
BAY 11-7085	Bio-Techne	Cat # 1743
Cycloheximide	Sigma-Aldrich	1810
DAPI	ThermoFisher	Cat# 62248
DharmaFECT1	Dharmacon	T-2005-01
GYKI-52466	Sigma-Aldrich	G119
ISH-23	Selleckchem	Cat # S7351
(N93	Sigma-Aldrich	K1385
MK801	Sigma-Aldrich	M107
	Sigma-Aldrich	P6500
Pentylenetetrazole (PTZ)	olgina Alanon	
• • • • • • • • • • • • • • • • • • • •	Thermo Fisher Scientific	Cat# P36970
ProLong Diamond AntiFade	· ·	Cat# P36970 L-059173-00-0005
ProLong Diamond AntiFade siRNA <i>α-Camk2a</i> SMARTPool	Thermo Fisher Scientific	
Pentylenetetrazole (PTZ) ProLong Diamond AntiFade siRNA α-Camk2a SMARTPool siRNA α-Creb1 SMARTPool siRNA Non-targeting Control Pool	Thermo Fisher Scientific Dharmacon	L-059173-00-0005

(Continued on next page)



Continued		
REAGENT or RESOURCE	SOURCE	IDENTIFIER
Critical commercial assays		
MultiTox-Fluor Multiplex Cytotoxicity Assay	Promega	Cat # G9201
Brilliant Calcium Flex	Ion Biosciences	10000-10
Adult Brain Dissociation Kit, mouse and rat	Miltenyi Biotec	Cat #130-107-677
Creb transcription factor assay kit (p-Ser133)	Cayman Chemical	Item No. 10009846
CellTiter-Glo 2.0 Cell Viability Assay	Promega	G9241
μMACS and MultiMACS DYKDDDDK Isolation Kits	Miltenyi Biotec	Cat #130-101-636
Quigen Rneasy Mini	Qiagen	#74106
qScript cDNA Synthesis kit	Quantabio	#95047
CycLex® CaM-kinase II assay kit	CycLex	Code # CY-1173
Caspace-3 Colorimetric assay kit	R&D Systems	Cat # K106-100
MultiTox-Fluor Multiplex Cytotoxicity Assay	Promega	Cat # G9201
Deposited data		
Microarray data	NCBI Gene Expression Omnibus	GEO: GSE122121
RNA sequencing data	NCBI Gene Expression Omnibus	GEO: GSE264436
Experimental models: Cell lines		
Vero E6	UTMB	N/A
Experimental models: Organisms/strains		
C57BL/6J	Jackson Laboratories	000664
Ripk3-/-	Genentech	N/A
Ripk3fl/fl	Genentech	N/A
Ripk3-2xFVfl/fl	Oberst Lab	N/A
Syn1 Cre	Jackson Laboratories	003966
Nestin Cre	Jackson Laboratories	003771
Mlkl-/-	Oberst Lab	N/A
Oligonucleotides		
See Tables S2 and S3		
Software and algorithms		
Prism version 10	GraphPad Software	graphpad.com; RRID:SCR_002798
Excel	Microsoft Corporation	microsoft.com/en-us/; RRID:SCR_016137
IPA	QIAGEN Silicon Valley	www.qiagen.com/us; RRID:SCR_008653
MATLAB	MathWorks	www.mathworks.com/; RRID:SCR_001622
QuPath	QuPath	qupath.readthedocs.io/en/0.5/; RRID:SCR_018257

EXPERIMENTAL MODELS AND STUDY PARTICIPANT DETAILS

Mouse lines

Ripk3^{-/-}, ⁸⁹ *Ripk3*^{fl/fl}, ³⁵ *Ripk3*-2xFV^{fl/fl}, ¹⁴ *Syn1*-Cre (JAX strain 003966), and *Nestin*-Cre (JAX strain 003771) mice in this study were bred and housed under specific-pathogen free conditions in Nelson Biological Laboratories at Rutgers University. All lines were congenic to the C57BL/6J background (JAX strain 000664). For most experiments using whole-animal knockout lines, heterozygus littermates were used as controls. We note that Ripk3^{+/-} and Mlkl^{+/-} animals do not exhibit haploinsufficiency and are routinely used as littermate controls in studies. ^{90–92} Primer sequences used to genotype all transgenic mouse lines are listed in Table S2. PCR was conducted using Platinum Taq DirectPCR and Lysis buffer (Invitrogen) using genomic DNA extracted from ear tissue following standard procedures. All mouse studies were performed in 8-12 week old animals of both sexes, following protocols approved by the Rutgers University Institutional Animal Care and Use Committee (IACUC). We did not observe any sexually dimorphic phenotypes in any of the experiments reported in this study.



Viruses and virologic assays

ZIKV strain MR766 was provided by the World Reference Center for Emerging Viruses and Arboviruses (WRCEVA). WNV strain WN02-Bird 114⁹³ was generously provided by Dr. Bobby Brooke Hererra (Rutgers Robert Wood Johnson Medical School). Vero cells (ATCC #CCL-81) were used to propagate the virus and maintain viral stocks. These cells were cultured in DMEM (Corning #10-013-CV) enriched with 10% heat-inactivated fetal bovine serum (FBS) (Gemini Biosciences #100-106), 1% penicillin-streptomycin-glutamine (Gemini Biosciences #400-110), 1% amphotericin B (Gemini Biosciences #400-104), 1% non-essential amino acids (Cytiva #SH30238.01), and 1% HEPES buffer (Cytiva SH30237.01). Viral titers were quantified using a plaque assay on the cultured Vero cells. The basal medium for the assay was 1X EMEM (Lonza #12-684F), supplemented with 2% heat-inactivated FBS, 1% penicillin-streptomycin-glutamine, 1% amphotericin B, 1% non-essential amino acids, 1% HEPES, 0.75% sodium bicarbonate (VWR #BDH9280), and 0.5% methyl cellulose (VWR #K390) to form the overlay medium. At 4 days post-infection, the overlay media was removed and cells were fixed/stained using 10% neutral buffered formalin (VWR #89370) and 0.25% crystal violet (VWR #0528) to visualize and count plaques.

Cell culture and infection

Primary cerebral cortical neurons were derived from E15 mouse embryos as previously described. ¹⁵ Neural tissue was harvested and processed using a Neural Tissue Dissociation Kit-T (Miltenyi, #130-093-231) using both male and female embryos. Neurons were seeded onto multi-well plates that had been pre-coated with 50μg/mL Poly-D-lysine (Thermo Fisher Scientific, #A3890401). Cultures were sustained in Neurobasal-Plus Medium (Thermo Fisher Scientific, #A3582901), enhanced with B-27-Plus supplement (Thermo Fisher Scientific, #A3582801). Cell culture viability and other assay experiments were performed at 14days *in vitro* (DIV) and RNA-seq at 21DIV. For ZIKV infection experiments, neuronal cultures were infected at a multiplicity of infection (MOI) of 0.1.

METHOD DETAILS

Transcriptomic analysis

Transcriptomic analysis was performed using two distinct data sets. The first was a microarray analysis previously published by us and others using primary cortical neuron cultures derived from both Ripk3^{+/+} and Ripk3^{-/-} mice infected with ZIKV-MR766 or WNV-TX for 24 hours (GEO accession number: GSE122121). The second was a new analysis derived from bulk-RNA sequencing of primary cortical neurons expressing RIPK3-2xFV. Neurons were treated with B/B or vehicle solution in the presence of KN93, 666–15, or control solution for 24 hours prior to harvest. Library preparation and Next Generation Sequencing was performed by Azenta Life Sciences (Piscataway, NJ). RNA yield and sample quality were assessed using Qubit (Invitrogen) and TapeStation (Agilent). Sequencing was performed on the Illumina HiSeq platform using 2 x 150-bp paired-end reads. Sequence reads were cleaned of adapters and low-quality sections, deduplicated, and aligned to the mouse reference genome via the STAR aligner. Gene expression quantification was carried out by counting unique sequences within gene exons. Differentially expressed genes were identified using DESeq2. The GEO accession number for this dataset is GSE264436.

Mouse infections and tissue harvesting

Intracranial infections were carried out by injecting 10 plaque-forming units (PFU) of ZIKV in 10 μ l of Hank's Balanced Salt Solution (HBSS) into the third ventricle of the brain. Subcutaneous infections were performed by injecting 10^3 PFU of WNV in 50 μ l of HBSS into the rear footpad. ZIKV infections were performed intracranially as wildtype mice are generally resistant to peripheral ZIKV infection, ^{94,95} while peripheral WNV infection with the North American strains used in our study is sufficient to induce clinical neurologic disease. ⁹³ For clinical monitoring, infected mice were weighed and observed daily for signs of disease, following established protocols. Mice were euthanized if they became moribund or lost more than 20% of their initial body weight. ¹⁴ At designated time points post-infection, mice were perfused with 30 mL of cold phosphate-buffered saline (PBS) or 4% paraformaldehyde (PFA) for tissue fixation, depending on the downstream analysis. PBS-perfused tissues were either processed for adult neuron isolation using magnetic-activated cell sorting (MACS) (Miltenyi Biotec, 130-126-602), used for protein pulldown with the Miltenyi μ MACS FLAG-protein isolation kit (Miltenyi Biotec, 130-101-591), or preserved in TRI Reagent (Zymo Research, #R2050-1) for gene expression analysis. Tissues perfused with 4% PFA were processed for immunofluorescence studies.

Cell Death Assays

Cell viability was evaluated using two distinct methods: the MultiTox Cytotoxicity Assay (Promega, G9201) and the ATP-based CellTiter-Glo Assay (Promega, G7573). The MultiTox Cytotoxicity Assay simultaneously measures live cell (AFC) and dead cell (R110) protease activities within each culture well, providing two complementary data points. AFC signal was normalized to group means of mock or vehicle controls within experiments, while R110 signal were normalized as a percentage of the maximum response observed among groups within a given experiment. The CellTiter-Glo Assay determines cellular ATP concentration, serving as an indicator of metabolically active cells. The luminescence output, reflective of ATP concentration, was normalized to group mean values for mock or vehicle controls. Both fluorescence and luminescence signals in these assays were quantified using a SpectraMax iD3 plate reader (Molecular Devices).





Diseases & Functions, Canonical Pathways, and Kinase Regulator Analysis

The Diseases & Functions, Canonical Pathways, and Kinase Regulator Analysis tools within the Ingenuity Pathway Analysis platform were used to identify biological functions, diseases, pathways, and upstream kinase regulators most significantly enriched in our transcriptomic datasets. Genes from the dataset that met the adjusted p-value cutoff of less than 0.05 and were associated with biological functions, diseases, canonical pathways, or kinase regulators in the QIAGEN Knowledge Base were used for analysis.

Fluorescent In Situ Hybridization (FISH)

FISH was performed as previously described. ⁹⁶ Briefly, tissue sections were air-dried and re-fixed in 4% paraformaldehyde (PFA) in PBS for 10 minutes at room temperature. Following fixation, slides were washed in PBS and then permeabilized with 1 mg/mL Proteinase K (ThermoFisher) for 20 minutes. After PBS washes, tissues were re-fixed in PFA and subjected to an ethanol dehydration series: 50%, 70%, and two rounds of 100% ethanol, followed by air drying for 5 minutes. Slides were then placed in probe hybridization solution for at least 10 minutes at 37°C. Probes specific for Ripk3 (Table S3, IDT DNA oPools) were added at a final concentration of 4 nM, and hybridization occurred overnight at 37°C. The next day, slides were washed sequentially in wash buffer and 5x SSCT (5x SSC with 0.1% Tween 20). After removing excess liquid, samples were incubated in amplification buffer at room temperature for 30 minutes before hairpin amplification, which proceeded overnight at room temperature. Finally, slides were washed in 5x SSCT, rinsed in 5x SSC, and mounted. We then proceeded with our immunohistochemistry protocol for neuron staining with NeuN.

Calcium Flux Assay

Calcium flux dynamics in primary cortical neuron cultures were evaluated using the Brilliant Calcium Flex kit (IonBiosciences, 10000), according to manufacturer's instructions. Briefly, following experimental treatments, neuron cultures were incubated with a cell membrane-permeable fluorogenic calcium sensor for 1h at 37° C. Cells were then stimulated with a pulse of 100μ M NMDA and fluorescent signal was recorded at 10-second intervals for a total duration of 60 seconds.

siRNA Transfection

Primary neurons were cultured in 96-well plates and transfected with siRNA pools targeting *Camk2a*, *Creb1*, or a scrambled non-targeting control, using DharmaFECT transfection reagent and following the manufacturer's protocol. A final siRNA concentration of 25 nM was used. siRNA and DharmaFECT reagent were diluted separately in serum-free medium, incubated for 5 minutes, combined, and further incubated for 20 minutes at room temperature. The transfection mixture was added to neurons in anti-biotic-free neurobasal medium. After 48 hours of incubation at 37°C with 5% CO₂, cells were processed for downstream analyses.

Chemical reagents

The following chemical reagents were used in cell culture experiments: GYKI-52466 (1μ M, Sigma, G119), MK801 (1μ M, Sigma, M107), GSK 872 (1μ M, Tocris, 6492), B/B Homodimerizer (200nM, Takara, 635058), L-Glutamic acid (100-1,000 μ M, Sigma, G1251), N-Methyl-D-aspartic acid (20μ M-100 μ M, Sigma, M3262), KN93 (1μ M, Sigma, K1385), myristoylated AIP (1μ M, Tocris, 5959), 666-15 (1μ M, Tocris, 5661), Actinomycin D (10 ng/ml, Sigma, A1410), Cycloheximide (1μ g/ml, Sigma, C7698), JSH-23 (50μ M, Selleckchem, S7351), BAY 11-7085 (100μ M, Tocris, 1743). For *in vivo* injections, the following chemicals were used: GYKI-52466 (1μ g/g), MK801 (0.06μ g/g), pentylenetetrazole (PTZ) (40μ g/g, Sigma, P6500), B/B Homodimerizer (10μ g/g).

Quantitative real-time PCR

Total RNA was extracted from primary neuron cultures using the Qiagen RNeasy Mini Kit (Qiagen, 74106), adhering to the manufacturer's protocol. RNA concentration was determined using a Quick Drop device (Molecular Devices). Complementary DNA (cDNA) was then synthesized using the qScript cDNA Synthesis Kit (Quantabio, 95047). Quantitative RT-PCR (qRT-PCR) was performed utilizing SYBR Green Master Mix (Bio-Rad, CA1725125) on a QuantStudio5 instrument (Applied Biosystems). Cycle threshold (CT) values for the genes under study were normalized to the CT values of the housekeeping gene 18S (CT_Target – CT_18S = Δ CT). Data were further normalized to baseline control values (Δ CT_experimental – Δ CT_control = Δ Δ CT (DDCT)). A list of primer sequences used in the study is provided in Table S2.

Immunofluorescence

Fluorescent immunocytochemistry (ICC) was performed following fixation of cells in 4% paraformaldehyde for 10 minutes. Cells were then blocked with 10% goat serum containing 0.1% Triton X-100 for 15 minutes. Primary antibodies were applied for 1 hour at room temperature, followed by secondary antibody incubation for 15 minutes. Nuclei were stained with DAPI at a 1:10,000 dilution for 10 minutes. Between each step, cells were gently washed with 1X PBS to remove unbound antibodies. Coverslips were mounted onto glass slides using ProLong Diamond Antifade Mountant (ThermoFisher, P36970).

For immunohistochemistry (IHC), mice were perfused with 30 mL of cold 1X PBS, followed by freshly prepared 4% paraformaldehyde in 1X PBS. Brains were stored at 4° C overnight, then transferred to 1X PBS until sectioning. Brains were embedded in agar and sectioned using a compresstome (Precisionary, VF-510-0Z). 40μ M free-floating sections were blocked with 10% goat serum containing 0.4% Triton X-100, followed by incubation with primary antibodies for 48 hours at 4° C. After washing, sections were incubated with secondary antibodies for 1 hour at room temperature and then stained with DAPI at a 1:1,000 dilution for 10 minutes. Sections were mounted onto glass slides using ProLong Diamond Antifade Mountant.



Primary antibodies used for ICC and IHC included rabbit anti-mCherry (1:100, Rockland, 600-401-P16), chicken anti-MAP2 (1:2,500, Abcam, ab5392), guinea pig anti-NeuN (1:500, Synaptic Systems, 266-004), phospho-CaMKIIα (1:500, ThermoFisher, PA1-4614), rabbit anti-phospho-CREB (1:100, ThermoFisher, MA5-11192), rat anti-GFAP (1:250, ThermoFisher, 13–0300), and chicken anti-S100b (1:500, SynapticSystems, 287006). Secondary antibodies were used at 1:250 dilutions: goat anti-chicken 488 (ThermoFisher, A-11039), goat anti-rabbit 488 (ThermoFisher, A32731), goat anti-rat 488 (ThermoFisher, A-11006), goat anti-rabbit 594 (ThermoFisher, A-11012), goat anti-guinea pig 594 (ThermoFisher, A-11076), and goat anti-pig 647 (ThermoFisher, A21450). Imaging was conducted using an Airyscan fluorescent confocal microscope (Carl Zeiss, LSM 800). Quantification of fluorescence was performed with QuPath v0.4.3 (QuPath, RRID:SCR_018257), an open-source software for digital pathology image analysis. DAPI-positive nuclei were detected using the cell detection command, and a cell classifier was applied against secondary cell markers (e.g., NeuN for neurons) based on fluorescence intensity thresholds. Signal intensity for target markers (e.g., mCherry, pCaMKII, pCREB) was extracted from individually classified cells.

Microelectrode array (MEA) recordings

MEAs (Multi Channel Systems, 60MEA200/10iR-Ti) consist of 59 titanium nitride (TiN) working electrodes with a diameter of 10 μm with 200 μm spacing between electrodes and one internal reference electrode. Prior to recording, MEAs were treated with oxygen plasma for 30 seconds using a PX-500 Plasma System (March Instruments), 100 μg/mL of poly-D-lysine overnight (Sigma, P0899), and 10 μg/mL Laminin (Sigma, L2020) for 2h prior to culture of primary neurons. For recording, culture medium was removed and 1 mL of warmed MEA recording solution 97,98 was added to each MEA. Each culture was allowed to equilibrate with the MEA solution for 5 minutes in the 37°C incubator before recording. Recordings were conducted with a MEA2100-Lite-System (Multi Channel Systems) that was maintained at 37°C using the TC02 temperature controller (Multi Channel Systems). The Multi Channel Experimenter software (Multi Channel Systems) was used to record the extracellular potential at each electrode for 5 minutes using a sampling rate of 20 kHz. After recording, MEA recording solution was removed and the conditioned cell culture medium was returned to the MEA.

MEA signal processing and analysis

All signal processing was conducted using MATLAB (Mathworks). All signals were filtered with a fourth-order Butterworth bandpass filter (300 – 3,000 Hz) to remove low frequency signals and a 60 Hz comb filter was used to remove noise generated by the hardware. ⁹⁹ An adaptive thresholding algorithm was used to detect 'spikes' in the extracellular recordings. For each 10 second interval on each working electrode, a threshold was defined as 4.5 standard deviations times the background noise of that time interval. Whenever the magnitude of the signal exceeded that threshold, a spike was recorded. A minimum interspike interval (ISI) of 2 msec ensured that the same spike was not recorded multiple times. Each electrode had a spike rate calculated as the number of recorded spikes in that channel per minute of recording. Fano factor, a measure of the distribution of spikes over the recording time, was calculated by dividing the recording time into 100 msec bins and counting the number of spikes per bin. The Fano factor was then calculated by dividing the variance of spikes per bin by the mean number of spikes per bin: $FF = \sigma_{bin spike count}^2/\mu_{bin spike count}$. The Brain Connectivity Toolbox (BCT)¹⁰⁰ was used to characterize network modularity and efficiency. For each electrode, we counted the number of spikes occurring in each 1 msec bin. Functional connectivity matrixes were generated by computing the cross-correlation between the binned spike-trains of each pair of working electrodes using a maximum lag-time of 20 msec. BCT functions for modularity, global efficiency, and local efficiency were then used to quantify those variables.

Seizure Assay

Seizures were induced by a single i.p. injection of pentylenetetrazole (PTZ) (Sigma-Aldrich, 54-95-5) at a dose of $40\mu g/g$ of body weight. Behavioral responses were evaluated using a modified version of the Racine scale as previously described. Adaptation of the scale included broader distinctions between myoclonic and clonic seizures and expanded criteria for generalized hypoactivity. Video recordings of mouse seizures were scored by an operator blinded to the experimental condition of each subject.

FLAG Pulldown and Western Blot

Pulldown of FLAG-tagged RIPK3-2xFV protein was conducted using the DYKDDDDK Isolation Kit (Miltenyi, 130-101-591) following the manufacturer's instructions. For Western blot analysis, primary antibodies against the following targets were used: RIPK3 (Cell Signaling Technology, 95702S), CaMKIIα (ThermoFisher, MA1-048), phospho-CaMKIIα (Thermo Fisher Scientific, PA1-4614), and Actin (Sigma-Aldrich, SAB3500350). Secondary antibodies included Goat anti-rabbit IRDye 800CW (Licor Biosciences, 925-32218), Goat anti-mouse IRDye 800CW (Licor Biosciences, 925-32210), and Donkey anti-chicken IRDye 680RD (Licor Biosciences, 926-68075). The immunoblots were visualized using the Odyssey XF Imaging System, which is equipped with two near-infrared lasers.



QUANTIFICATION AND STATISTICAL ANALYSIS

Statistical analyses were performed using GraphPad Prism 9. Survival experiments were compared via log-rank test. Most other experiments were compared with appropriate parametric tests, including the Student's t-test (two-tailed) or two-way analysis of variance (ANOVA) with Tukey's post hoc test to identify significant differences between groups. A p-value of less than 0.05 was deemed to indicate statistical significance. Unless specified otherwise, all data points represent biological replicates consisting of distinct mice or independent cultures derived from distinct mice.

Supplemental information

The kinase RIPK3 promotes neuronal survival by suppressing excitatory neurotransmission during central nervous system viral infection

Irving Estevez, Benjamin D. Buckley, Marissa Lindman, Nicholas Panzera, Tsui-Wen Chou, Micheal McCourt, Brandon J. Vaglio, Colm Atkins, Bonnie L. Firestein, and Brian P. Daniels

Supplemental Material

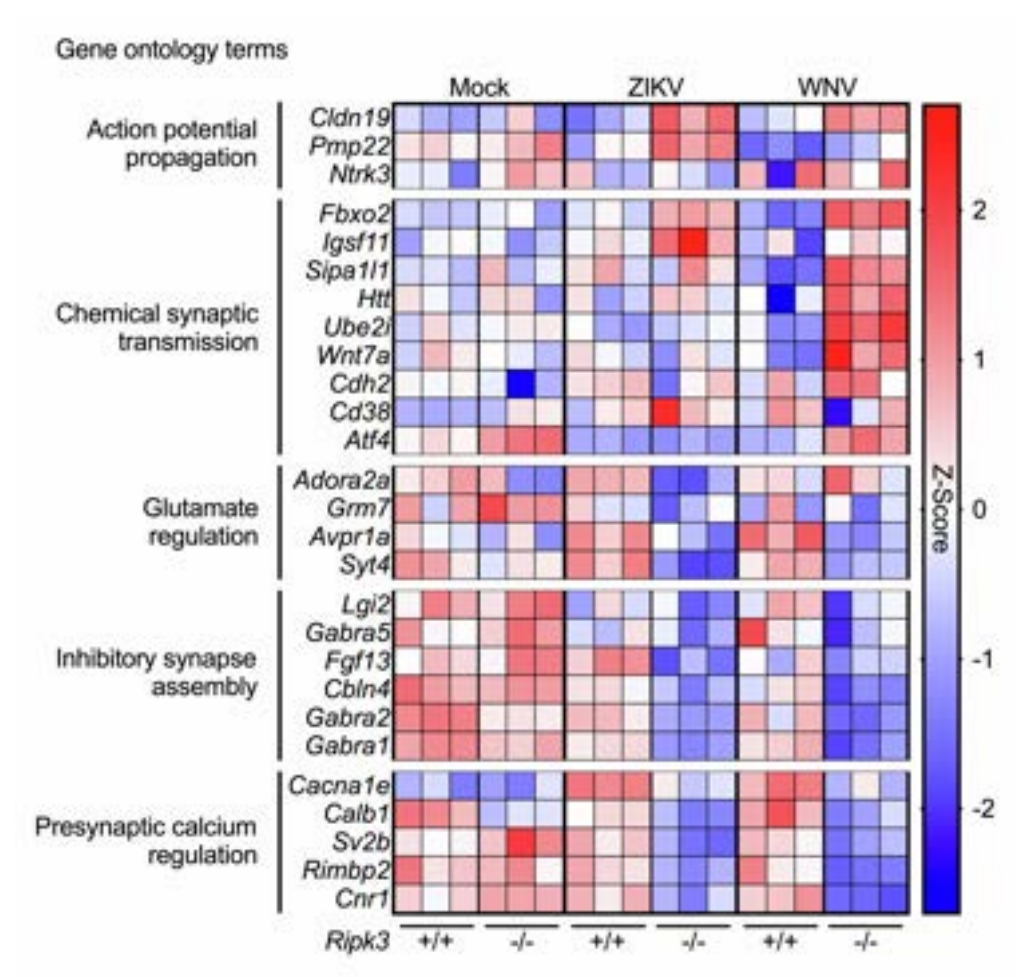


Figure S1. Heat map of genes representing major neurobiological GO terms in *Ripk3*^{-/-} and *Ripk3*^{+/+} neurons following ZIKV and WNV infection. Related to Figure 1.

Heat map illustrates the relative expression levels of genes associated with action potentials, synaptic transmission, glutamate and calcium regulation, and inhibitory synapse assembly. Genes were selected based on their involvement in neurobiological processes identified in GO term analysis, highlighting differences between *Ripk3*-/- and *Ripk3*-/- neurons across both viral infection groups.

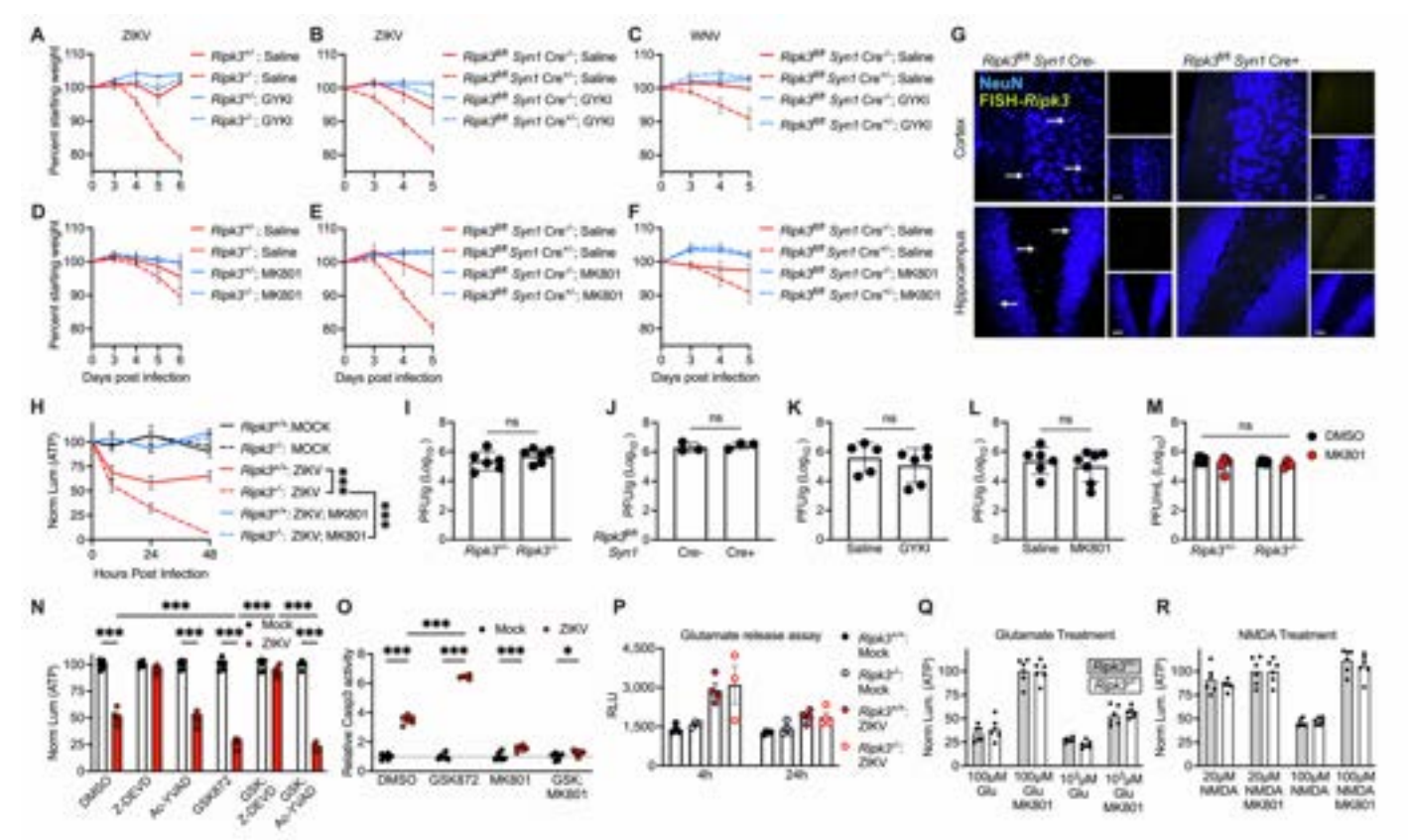


Figure S2. Basal effects of GluR inhibitors and *Ripk3*-deficiency on viral burden, viral replication, glutamate release, mechanisms of cell death, and excitotoxicity. Related to Figure 2.

- (A-F) Weight loss in mice of indicated genotypes following ZIKV intracranial infection (A-B, D-E) or WNV footpad infection (C, F) and 5 days of daily intraperitoneal administration of indicated glutamate receptor inhibitors.
- (G) Colocalization validation of *Ripk3* excision in *Ripk3* fl/fl *Syn1* Cre⁺ mouse brains using fluorescence in situ hybridization (FISH) targeting *Ripk3* mRNA (yellow) and neuronal marker NeuN (blue) in the cortex and hippocampus. Scale bar: 50 microns.
- (H) ATP-based viability assay (CellTiter Glo) assessing the effects of glutamatergic signaling on neuronal survival in primary neuron cultures from indicated genotypes following ZIKV infection. N = 6 independent cultures per group/condition.
- (I-L) Viral titer measurements via plaque assay in whole brain homogenates at 4 days post-infection, comparing whole-body *Ripk3*^{-/-} versus *Ripk3*^{+/-} (I), neuron-specific *Ripk3*^{fl/fl} *Syn1* Cre⁺ versus *Ripk3*^{fl/fl} *Syn1* Cre⁻ (J), and ZIKV-infected B6/J mice treated with either GYKI-52466 (K) or MK801 (L).
- (M) Plaque assay measuring viral titers in the supernatant of *Ripk3*^{+/-} versus *Ripk3*^{-/-} neuron cultures pretreated with MK801 and infected with ZIKV for 24 hours.
- (N) ATP-based viability assay evaluating the impact of various inhibitors on cell death mechanisms in WT primary neuron cultures following ZIKV infection. N = 6 independent cultures per group/condition.
- (O) Caspase 3 activity assay (R&D Systems) in WT primary neurons following ZIKV infection, with indicated inhibitor pretreatments. N = 6 independent cultures per group/condition.
- (P) Glutamate release assay (Glutamate-Glo) in cortical neuron cultures of indicated genotypes at 4 and 24 hours following ZIKV infection.
- (Q-R) ATP-based viability assays evaluating basal sensitivity to different concentrations of glutamate (Q) and NMDA (R) in cortical neuron cultures of specified genotypes, with MK801 used as a control for NMDAR antagonism.

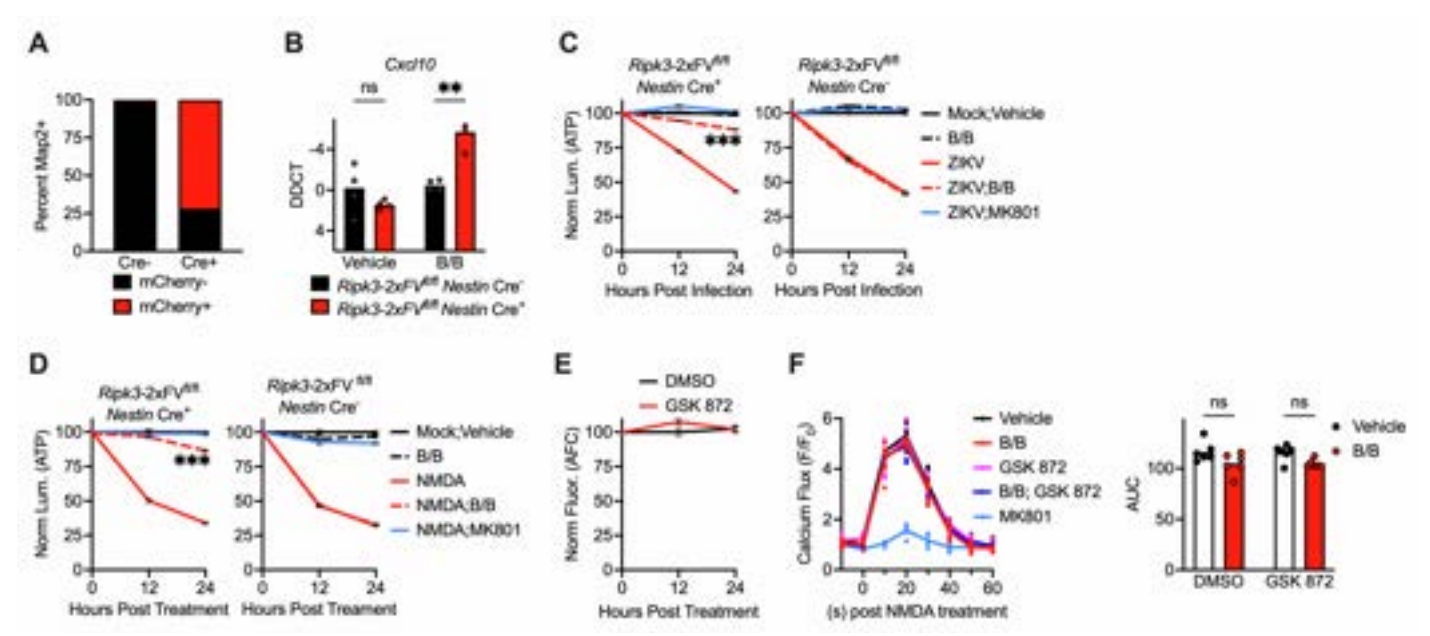


Figure S3. Impact of chemogenetic RIPK3 activation on *Cxcl10* expression, neuronal viability, and calcium flux dynamics. Related to Figure 3.

- (A) Percentage of MAP2⁺ neurons expressing mCherry in primary cortical neuron cultures from Ripk3- $2xFV^{fl/fl}$ Nestin Cre^- or Cre^+ as shown in Figure 3B.
- (B) Measurement of *Cxcl10* transcript levels via qRT-PCR in *Ripk3*-2xFV^{fl/fl} *Nestin* Cre⁺ and Cre⁻ neuron cultures after 24h of B/B treatment.
- (C-D) ATP-based viability assays (CellTiter Glo) assessing the impact of 24h B/B pretreatment on primary neuron cultures of indicated genotypes post-ZIKV infection (C) or NMDA exposure (D). N = 6 independent cultures per group/condition.
- (E) MultiTox cell viability assay evaluating the effects of the RIPK3 inhibitor GSK 872 on basal neuron viability in WT neuron cultures, measured using live cell protease activity (AFC). N = 6 independent cultures per group/condition.
- (F) NMDA-evoked Ca²⁺ dynamics in cortical neuron cultures following 2h pretreatment with specified drugs, measured at 10-second intervals in the presence of Brilliant Calcium Flex reagent. Area under the curve (AUC) analysis comparing indicated groups.
- **p < 0.01, ***p < 0.001. Error bars represent SEM.

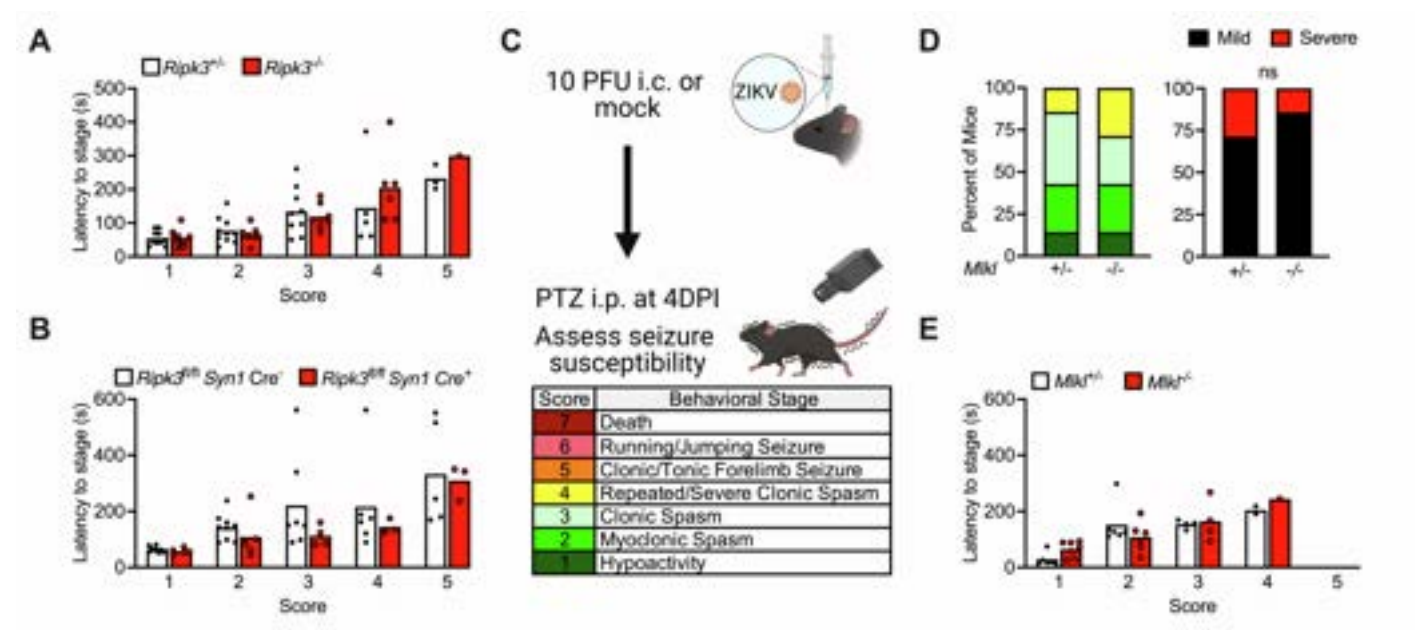


Figure S4. PTZ-induced seizure latency in mock-infected mice; MLKL does not affect PTZ-induced seizures during flavivirus infection. Related to Figure 4.

- (A-B) Latency time in seconds for mock-treated mice to reach consecutive seizure stages as shown in panel (Fig 4D-E).
- (C) Schematic depicting the protocol for inducing seizures with pentylenetetrazol (PTZ) 4 days after intracranial ZIKV infection or mock control, including a table explaining the modified Racine Scale of murine seizure stages.
- (D) Proportion of mice reaching indicated behavioral seizure stages, with "severe" seizures defined as stage 4 or higher, across indicated genotypes. N = 6-7 mice/group.
- (E) Latency time in seconds for mice to reach consecutive seizure stages as shown in panel (D).

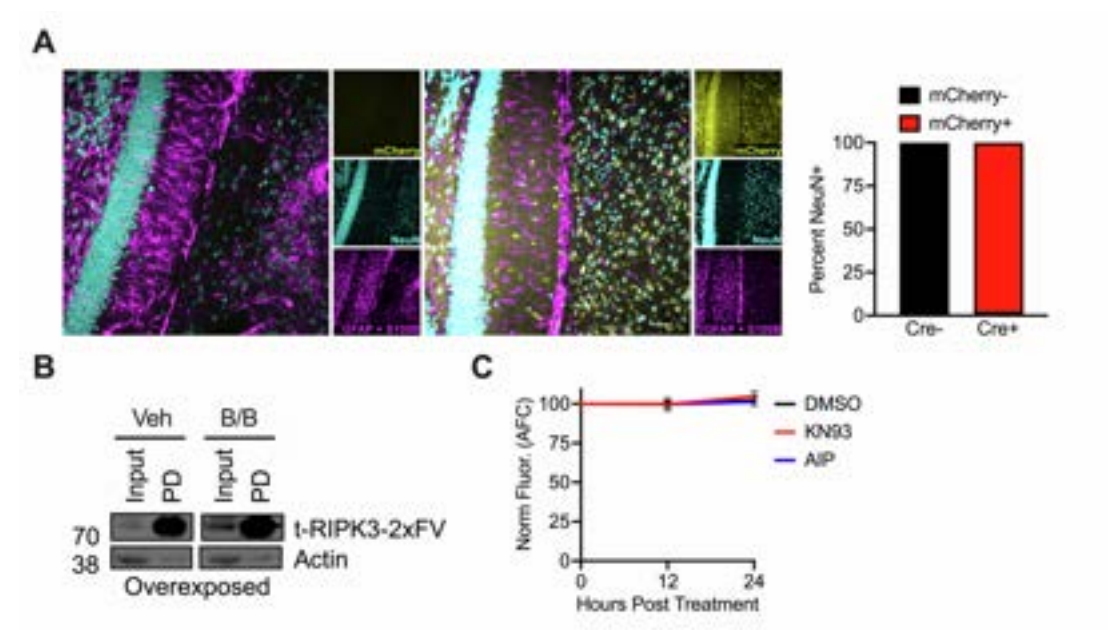


Figure S5. Confirmation of RIPK3-2xFV expression in transgenic mouse line and pulldown assays. Related to Figure 5.

- (A) Immunohistochemistry validation of *Ripk3*-2xFV^{fl/fl} *Syn1* Cre mouse line. Fixed brain tissue stained for the RIPK3-2xFV transgene reporter marker mCherry (yellow), neuronal marker NeuN (cyan), and double-stained for astrocyte markers GFAP and S100B (magenta). Quantification represents the percentage of NeuN⁺ neurons expressing mCherry between Cre⁻ and Cre⁺ mice. Quantification was performed using QuPath software. Scale bar: 50 microns.
- (B) Overexposure of western blot shown in Figure 5B confirming RIPK3-2xFV expression in input samples. Actin is used as a loading control.
- (C) MultiTox cell viability assay evaluating the effects of the CaMKII inhibitors KN93 and AIP on basal neuron viability in WT neuron cultures, measured using live cell protease activity (AFC). N = 6 independent cultures per group/condition.

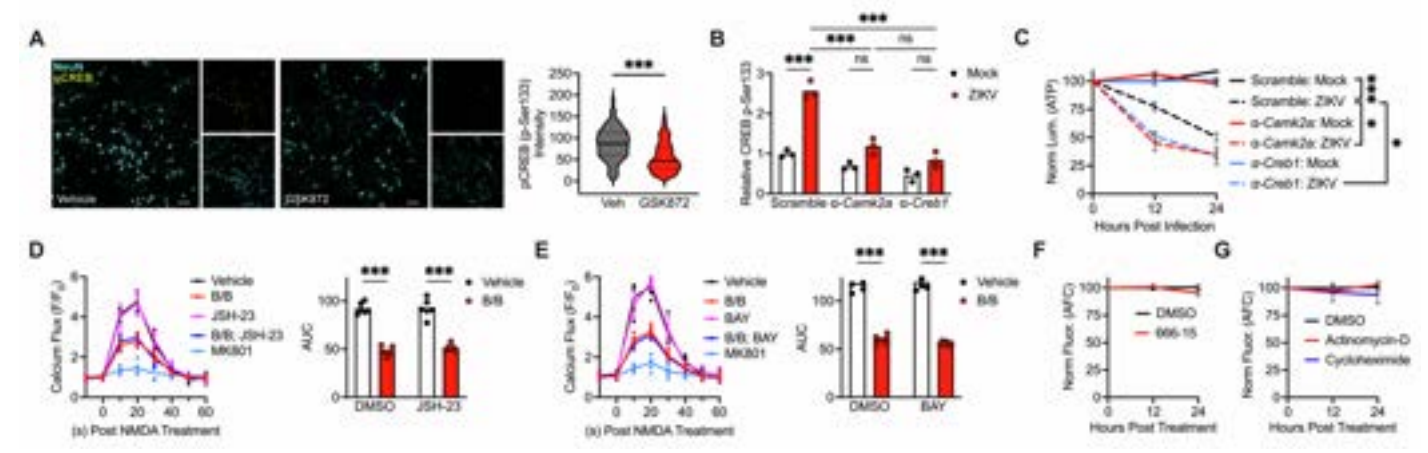


Figure S6. The neuroprotective effects of RIPK3 activation do not require NFkB but do require de novo transcription and translation. Related to Figure 6.

- (A) Immunocytochemistry on primary WT cortical neurons pre-treated with either GSK 872 or vehicle, followed by 24 hour ZIKV infection. Neurons were stained for NeuN (cyan) and phospho-Ser133 CREB (yellow), and pCREB signal intensity in NeuN⁺ cells was quantified using QuPath software. Scale bar: 50 microns.
- (B) CREB activation in ZIKV-infected primary cortical neurons following siRNA knockdown of *CaMKIIa* or *Creb1*. pCREB levels were quantified via an ELISA-based assay 24 hours post infection. N = 3 independent cultures per group/condition.
- (C) ATP-based viability assay (CellTiter Glo) showing the effects of $CaMKII\alpha$ or Creb1 knockdown on neuronal survival up to 24 hours post-ZIKV infection. N = 4 independent cultures per group/condition. (D-E) NMDA-evoked Ca^{2+} dynamics in cortical neuron cultures following 24h pretreatment with B/B and specified inhibitors of NF κ B, measured at 10-second intervals in the presence of Brilliant Calcium Flex reagent. Area under the curve (AUC) analysis comparing indicated groups. N = 6 independent cultures per group/condition.
- (F-G) MultiTox cell viability assay evaluating the effects of the indicated inhibitors of CREB (D) or transcription/translation (E) on basal neuron viability in WT neuron cultures, measured using live cell protease activity (AFC). N = 6 independent cultures per group/condition. *p < 0.05, ***p < 0.001. Error bars represent SEM.

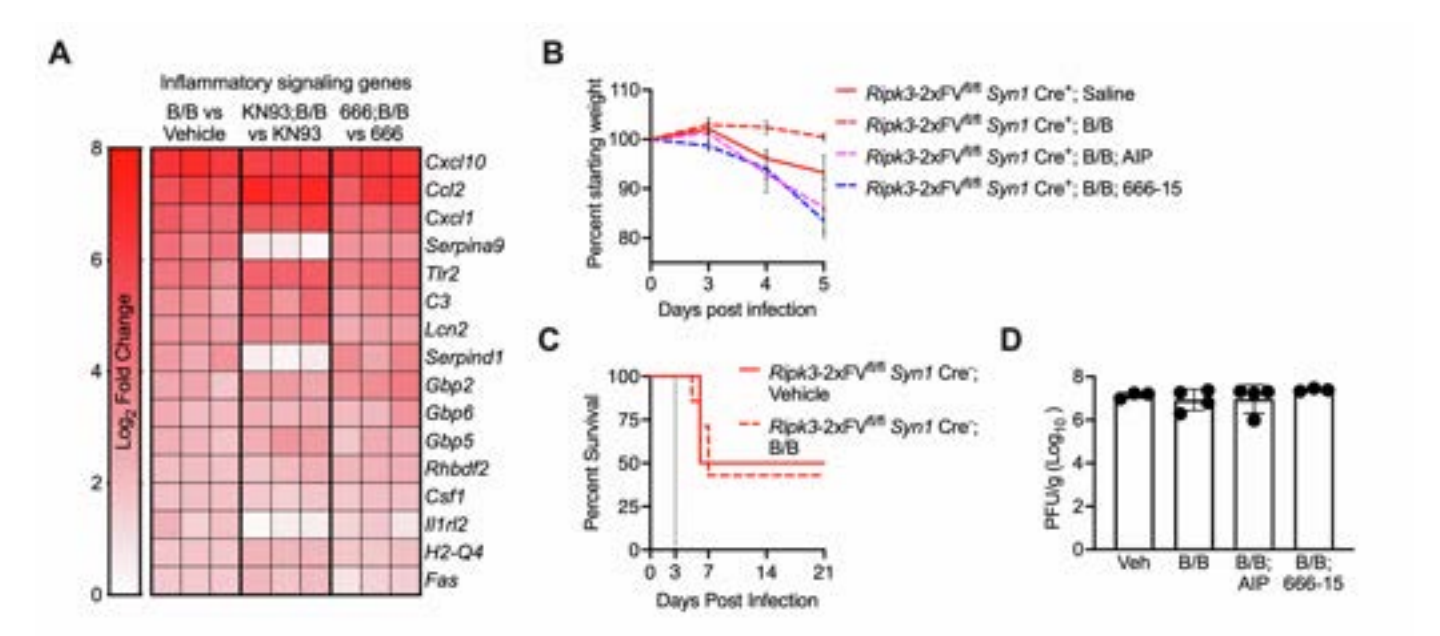


Figure S7. CaMKII and CREB are not required for RIPK3-dependent induction of inflammatory genes in neurons. Related to Figure 7.

- (A) *Ripk3*-2xFV^{fl/fl} *Nestin* Cre⁺ primary neuron cultures were treated with B/B or ethanol vehicle in the presence of KN93, 666-15, or DMSO vehicle for 24h and then subjected to bulk RNA-sequencing. Heatmap shows selected significant DEGs associated with inflammatory signaling. Data are expressed as Log₂ fold change values within each comparison.
- (B) Weight loss in *Ripk3-*2xFV^{fl/fl} *Syn1* Cre⁺ mice following ZIKV intracranial infection and intracranial administration of indicated drug a day 3 post infection. N=5-8 animals/group.
- (C) Survival analysis of mice in indicated treatment groups. All mice are Cre⁻ littermate controls of animals used in Figure 7J. N=6 animals/group.
- (D) Viral titer measurements via plaque assay in whole brain homogenates at 5 days post-infection in the presence of indicated CREB inhibitor.

Table S1. Seizure and epilepsy related genes shown in Figure 4B with z-Scores, Related to Figure 4

Ripk3^{-/-} Mock Ripk3-/- WNV **GENES B6/J Mock B6/J ZIKV** Ripk3-/-ZIKV **B6/J WNV** Snta1 -0.44 -0.89 -0.28 -0.98 -0.27 1.60 -1.14 -0.75 -1.13 0.50 0.25 Adk -0.81 -1.26 -1.27 -1.01 -0.35 -0.42 -0.77 -0.32 0.01 1.88 1.10 1.57 -1.23 0.16 0.15 0.53 1.07 0.98 Gabrb1 -0.34 -1.11 -1.17 -0.13 0.40 -0.10 -0.40 -0.92 -0.30 1.93 1.17 1.25 -0.39 -1.69 -0.87 1.04 0.50 1.14 1118 -1.08 -1.03 -1.14 -1.16 -0.45 -0.84 -0.81 -0.62 -0.59 0.35 -0.16 0.07 1.17 0.93 1.58 1.07 1.62 1.10 Ppt1 -1.06 -0.51 -1.25 -0.97 -0.37 -0.11 -0.62 0.22 -0.52 1.69 0.52 0.90 -0.39 -1.76 0.63 1.30 1.57 0.72 Fcqr3 0.00 -0.33 0.24 -0.53 -0.50 0.18 -1.18 0.37 -0.87 1.14 0.93 1.38 -0.90 -2.46 -0.34 1.09 0.66 1.13 Myd88 -1.07 -1.06 -0.63 -0.67 -0.23 1.66 2.12 -0.88 -0.67 -0.54 -0.62-0.59 0.00 -0.31 0.03 1.04 0.89 1.53 **Dhdds** -0.36 -0.72 -0.56 -1.38 -0.95 -0.22 0.76 0.45 1.04 1.28 -0.83 -0.70 1.30 0.88 1.52 0.83 -1.54 -0.80 Gfap -0.67 -1.09 -1.56 -0.30 0.02 0.19 0.29 -0.76 -0.18 1.10 1.14 0.64 -0.24 -1.83 -0.43 1.34 0.45 1.90 Fcgr2b -0.29 -0.58 -1.03 -0.48 0.83 0.79 -1.99 -0.51 -1.03 1.51 0.93 0.32 -0.99 1.12 -0.74 0.28 Fos -0.84 -0.81 -1.74 0.59 -1.15 -1.32 1.72 0.62 -0.78 0.31 1.47 1.23 -0.370.57 -0.470.76 0.45 -0.25 Pcmt1 -0.61 -1.31 -1.84 -0.95 0.62 0.01 -0.83 -0.32 -0.41 1.18 0.66 0.59 0.01 2.07 1.19 -0.97 0.34 0.57 Pign -0.91 0.01 -0.85 -0.48 -1.19 -1.30 0.22 -0.57 -0.31 0.84 0.98 -0.36 1.53 -1.39 -0.09 1.70 1.51 0.67 Abhd6 0.20 -1.00 -1.09 0.18 0.69 1.41 -0.95 -1.18 -0.43 1.25 0.91 2.00 -1.01 -1.00 -0.38 -0.10 -0.48 0.98 Atp6v1a 0.22 0.52 -0.19 -1.03 0.73 0.44 -0.44 -0.11 -0.63 1.12 1.31 0.44 -0.15 -2.81 0.31 0.57 -1.32 1.00 **Tiparp** -0.77 0.47 0.31 -1.98 0.07 -1.66 -0.48 1.06 0.06 -0.78 -1.14 1.53 0.60 0.06 1.43 -0.28 0.47 1.04 Fbxo33 0.29 -1.21 -1.99 -0.75 -0.45 -1.07 -0.35 -0.58 0.62 0.65 -0.01 -0.18 0.25 -0.12 0.97 0.12 2.00 1.81 Ctsd 0.55 0.90 0.66 0.30 -0.03 -0.06 -0.21 0.01 -0.08 0.66 0.62 0.93 -1.07 -3.11 -1.41 0.10 0.75 0.49 Gabra4 0.32 -0.35 2.06 0.49 0.23 -0.54 -0.14 -0.22 1.16 1.17 -1.19 -0.58 -1.91 -1.06 0.51 0.44 0.83 0.97 -2.31 -1.73 -0.60 Parp1 0.51 -0.39 -0.76 -0.18 1.01 0.23 0.43 0.80 1.09 -1.36 0.50 Cxcr4 -1.91 -1.42 -1.72 0.98 0.27 1.22 1.37 -1.16 -0.68 0.38 0.58 -1.12 Rgs2 0.19 -0.74 -0.61 -0.71 0.04 -1.37 -1.46 0.07 -0.33 -0.14 0.85 0.89 1.59 1.14 1.74 0.91 -0.95Otud6b -0.30 -0.97 -0.78 0.29 1.77 1.23 -1.18 -1.20 -0.66 1.05 0.42 1.45 -1.21 -0.89 0.98 -0.43 -0.30 0.70 Snx27 -0.94 0.17 -0.58 0.00 1.29 1.19 -0.09 -0.30 -0.35 0.93 0.82 0.66 0.08 -1.69 1.26 -1.47 -1.79 0.81 Gabrb3 -0.49 -1.00 -0.63 -0.27 -0.11 0.66 1.15 0.44 -0.08 1.28 0.67 0.01 0.60 -0.76 -1.86 -1.51 -0.24 2.13 Yipf5 -0.59 -0.03 -2.11 0.06 1.61 0.28 -0.79 -2.04 0.00 0.31 0.37 0.92 0.08 -0.69 1.57 -0.05 0.28 0.82 Slc1a3 -0.94 -1.21 -1.58 0.83 1.65 1.17 -0.98 -0.60 -0.47 0.99 0.37 0.71 -0.89 -0.91 -0.64 0.74 0.72 1.05 Impa1 -0.04 -0.34 0.19 -0.83 1.21 0.71 -1.70 0.77 -0.86 0.86 0.43 0.34 0.69 0.49 1.25 -0.99 -2.38 0.19 Crem -1.36 -1.57 -1.94 -0.62 0.73 1.23 1.52 -0.80 0.49 0.70 -0.38 0.15 -0.18 1.13 0.63 0.79 -0.55 0.04 0.41 -1.07 -0.40 -0.31 0.41 -0.58 -1.12 -0.55 -0.83 -0.42 -0.86 App -0.26 0.01 0.21 2.18 2.44 -0.20 0.95 -0.93 -0.79 -0.79 -0.67 -0.43 -0.57 1.46 Nampt -0.82 -0.90 -0.78 -0.26 -0.19 -0.89 1.21 0.90 1.48 1.42 1.53 Lgi1 -0.88 -0.47 -0.77 0.48 1.67 -1.27 -1.05 -0.27 -0.37 1.11 1.00 -0.31 1.73 0.68 -0.23 Npy -0.48 -0.24 0.03 1.57 2.15 1.62 -1.40 -0.69 -1.48 0.51 0.07 0.21 -0.95 -0.78 -0.530.25 0.38 Mapt -0.73 -0.18 -0.45 -1.15 -0.67 -0.91 1.84 0.42 0.97 0.41 -0.01 -0.36 0.67 1.50 1.55 -0.84 -1.69 -0.38 Ppp3cb -0.58 -0.51 0.01 -1.37 0.56 -0.35 0.53 0.35 0.48 0.80 -0.87 -0.18 -0.40 2.29 1.33 -2.11 -0.43 0.45 Cacna1e -0.79 -0.38 -1.35 -0.95 -1.39 -0.29 1.35 1.24 1.25 0.17 -0.63 -0.35 0.68 1.51 1.34 -0.83 0.24 -0.83 Akt3 -0.17 -0.03 -0.96 -0.27 0.36 -0.33 1.27 -0.48 0.39 0.37 -0.18 -0.59 2.35 -1.69 1.69 -0.17 -1.39 -0.19 Nbea -1.25 0.15 -0.44 -0.94 -0.92 -0.85 -1.30 0.82 0.55 1.36 -0.27 -0.59 -0.11 0.22 2.35 1.43 0.24 -0.46 Pde4dip -0.27 0.64 0.23 0.91 0.88 0.15 -1.08 0.07 1.04 -0.27 -0.93 0.25 -0.08 -0.98 1.13 1.30 -2.76 Snap91 0.32 -1.02 -1.14 0.17 -1.02 -0.85 -0.59 -0.87 -0.31 1.36 -0.21 1.05 -0.04 0.45 2.40 1.33 -0.92 -0.11 Cyfip2 -0.58 -0.31 -0.47 -0.83 0.55 1.34 0.28 0.74 -0.38 -0.17 0.51 -0.33 0.83 -2.30 1.81 -1.62 0.70 Rhobtb2 -0.21 -0.72 -0.25 -0.78 1.64 0.75 0.97 0.74 1.04 -0.74 -0.36 -1.13 -0.98 -0.60 -0.29 -1.10 -0.29 2.30 Tsc1 1.35 -0.50 1.18 -2.03 0.75 -0.19 0.58 0.65 0.67 0.61 -0.75 -0.36 Kcnc2 -1.23 -0.36 0.74 -0.87 -0.61 0.86 1.22 0.80 -0.38 -0.68 -0.49 -0.11 1.88 1.70 -1.10 -0.27 0.37 -1.46Atp1a3 0.16 0.62 -0.39 1.23 -1.86 -1.23 1.70 0.64 0.84 0.58 -0.84 -0.75 1.52 -0.64 -0.05 0.07 -0.37 -1.21 Enc1 -0.07 -0.97 -0.92 -0.77 -0.55 -1.15 1.57 0.97 1.48 -0.36 -0.97 -0.67 0.36 1.62 1.37 -0.92 -0.46 0.44 Tgm2 -1.20 -0.80 -0.72 -0.23 -0.85 -0.85 -0.03 0.75 0.32 -1.01 -0.60 -1.01 1.97 0.74 0.97 0.72 -0.15 1.98 Tbc1d24 0.37 0.38 1.42 -0.16 -0.76 -0.43 0.94 1.46 1.09 -0.16 0.04 -0.49 -1.48 0.84 0.91 -1.81 -0.91 -1.27 Plat 1.66 0.05 -1.04 -0.76 -0.23 -1.04 -0.86 -0.24 -0.39 0.95 0.71 -0.26 -1.28 -0.31 1.66 -1.16 1.14 1.38 Scn1a -0.59 0.36 -0.32 -0.11 -0.49 -1.14 0.57 0.72 1.77 -1.51 0.17 -0.97 1.01 2.38 -0.26 -0.29 -0.62 -0.66 Slc6a13 0.98 0.67 1.24 0.86 -0.49 0.92 1.05 -1.29 -1.34 -1.12 1.08 -0.57 -0.89 -0.98 0.67 1.03 -0.92 -0.90 Grm5 -0.25 -0.54 -0.92 0.47 0.74 0.35 -1.35 -0.23 -0.30 -0.38 0.42 1.27 1.56 -0.47 -0.94 -0.81 2.41 -1.01 Ntrk2 0.45 0.81 -0.61 -0.11 0.81 0.00 -0.88 1.01 1.39 0.98 -0.05 -0.32 -0.35 -0.94 -3.01 0.24 0.14 0.44 Adgrv1 1.51 -0.60 0.12 -1.00 -0.62 -1.23 -0.12 -0.14 0.81 -1.76 -1.02 1.28 1.84 0.99 0.12 0.12 -0.14 Scn3a 0.16 -0.32 -1.32 -0.30 0.82 1.37 0.81 0.35 -1.74 -0.45 -0.30 2.22 0.49 -0.02 -1.79 0.00 0.16

Grin2b	-0.35	0.67	0.64	1.64	0.37	1.02	0.47	-0.41	-0.69	-0.49	-0.07	-0.91	0.01	-2.55	-1.38	1.21	0.27	0.56
Plk2	-0.01	-0.35	0.07	-1.04	-1.27	-0.83	0.80	0.25	1.34	-0.79	-1.35	-1.20	0.54	1.93	1.61	-0.46	0.39	0.38
Gls	-0.97	-0.08	-0.28	-0.20	-1.33	-1.13	0.83	0.36	0.11	-1.16	-1.22	-1.00	1.04	1.43	0.42	1.73	1.39	0.07
lgsf9	-0.53	0.27	-1.15	-0.78	0.39	0.85	0.41	-0.06	0.68	-0.61	-0.78	-1.00	1.69	-1.97	-0.40	0.14	1.10	1.75
Gabra3	-0.33	0.80	0.02	-0.48	2.07	-1.10	-0.22	-0.15	0.38	-0.69	-1.54	-0.72	0.90	0.67	2.16	-0.59	-0.68	-0.48
Itpr1	0.96	0.44	0.43	-0.91	-0.81	-1.58	0.38	1.03	0.64	-0.77	-1.55	-1.02	0.81	1.88	1.00	-0.94	0.02	-0.01
Lingo1	0.17	0.65	0.81	1.32	0.61	-0.16	0.91	1.12	0.74	0.31	-0.12	0.01	0.02	-0.64	-0.49	-1.76	-2.51	-0.99
Elavl3	0.80	1.26	1.32	0.38	0.95	-1.12	-0.11	1.14	0.98	-0.91	-0.60	0.07	-0.40	0.70	-1.35	-1.42	-1.67	-0.02
Micall1	1.22	1.54	0.64	0.64	-1.64	0.07	0.84	0.29	0.49	-1.26	-0.43	-0.93	-0.67	0.58	-1.51	0.71	0.75	-1.35
Kcnv1	0.07	0.45	-0.29	-0.86	1.58	-0.41	1.35	1.36	0.81	-0.86	-0.46	-1.21	1.12	-1.28	1.02	-1.42	-0.18	-0.76
Nid1	0.85	0.80	0.88	-1.08	-0.62	-0.60	0.87	0.89	0.87	-0.75	-0.95	-0.97	1.01	1.08	1.30	-1.44	-1.12	-1.02
Grm7	0.99	-0.47	0.88	1.91	0.97	1.11	0.50	-0.33	-0.40	-1.72	-0.70	-0.01	-0.86	0.97	-1.06	0.07	-1.54	-0.32
Ank3	-0.69	1.27	-0.05	-0.99	0.74	-0.22	0.24	0.99	1.22	-0.74	-1.99	-0.67	-0.72	1.68	0.37	1.10	-0.84	-0.70
Gng7	-0.42	0.65	-0.48	0.39	1.32	-0.67	1.08	1.20	1.48	-1.05	-0.27	-1.31	1.55	-0.46	-0.26	-1.26	-1.37	-0.13
			-														<u> </u>	
Cplx1	-0.91	0.78	1.15	-0.05	1.02	-0.69	0.25	0.91	0.38	-1.22	-0.68	-1.12	0.91	1.01	1.50	-1.68	-1.17	-0.40
Dmxl2	0.15	0.99	1.42	1.78	-0.50	0.98	1.20	0.41	0.47	-0.43	-0.45	-0.88	-0.56	-0.58	-1.32	0.19	-1.30	-1.57
Ncam1	1.65	0.64	0.46	0.57	0.74	-0.62	0.64	0.08	-0.11	-2.62	-1.10	-0.14	-0.29	-0.86	-1.04	1.29	0.19	0.52
Gria1	-0.02	0.59	0.60	1.55	-0.90	0.85	1.11	0.21	0.17	-2.10	-1.05	-0.50	-0.16	-0.47	-1.66	1.38	0.60	-0.21
Rbfox1	0.78	0.24	0.61	-0.48	-0.09	-0.59	0.98	1.50	1.25	-0.75	-1.20	-1.45	-0.15	1.51	0.91	-1.39	-0.99	-0.69
Gdnf	2.58	0.35	-0.29	-0.51	0.46	0.08	0.73	0.86	0.61	-1.49	-1.63	-0.98	0.26	0.56	0.26	-0.09	-1.19	-0.57
Cacna1h	-0.14	0.77	0.52	1.85	0.58	0.83	-0.28	0.35	-0.44	-2.42	-1.13	-0.59	0.07	0.38	-1.68	0.83	0.32	0.18
Ngfr	0.94	0.55	0.63	-0.45	-0.01	-0.45	0.25	-0.37	-0.11	-1.85	-0.51	-1.37	0.64	2.78	-0.45	0.58	-0.76	-0.04
Ldlr	-0.59	-0.06	0.00	-0.13	-0.08	-0.16	0.73	1.09	1.16	-1.02	-1.02	-1.49	1.39	1.87	1.01	-1.33	-0.48	-0.90
Cacna2d2	0.56	1.55	0.68	0.44	2.33	0.05	-0.53	1.04	-0.25	-1.43	-1.09	-1.64	-0.08	-0.55	-0.54	-0.43	0.08	-0.20
Ryr3	1.18	1.58	0.33	1.26	0.61	-0.36	0.79	-0.19	-0.01	-1.08	-0.82	-1.03	0.95	0.83	-0.10	-1.16	-0.83	-1.94
Cdkl5	-0.48	-0.34	-0.06	0.31	0.44	0.79	-0.95	-0.09	0.32	-0.98	-1.14	-2.03	0.86	1.69	1.91	0.14	-0.90	0.53
Kcnt2	0.25	0.44	0.40	1.77	0.92	2.03	0.80	0.28	0.39	-1.09	-1.26	-0.20	-0.29	-0.29	-0.53	-1.10	-1.23	-1.28
Syn3	0.44	1.21	0.95	1.13	-0.09	-0.67	0.97	1.74	0.94	-1.18	-0.89	-0.88	0.69	-1.04	-0.45	-0.42	-1.33	-1.11
Cacna1b	2.02	-0.16	0.29	0.77	-0.27	1.86	0.66	0.36	0.43	-0.79	-1.66	-1.45	0.61	-0.29	-0.05	-0.50	-1.02	-0.83
Prdm8	0.36	0.37	0.09	0.49	0.63	-0.53	1.44	0.42	1.39	-0.56	-1.04	-1.69	0.21	1.14	0.84	-1.96	-1.10	-0.50
Gng3	0.09	1.03	0.29	-0.27	0.75	0.08	0.97	0.84	0.75	-0.37	-1.76	-1.05	0.65	0.74	0.78	-2.41	-1.14	0.04
Sv2b	0.33	0.03	0.09	0.55	2.09	1.17	0.86	0.18	0.55	-0.76	-1.47	-1.58	0.70	0.40	0.10	-1.54	-1.01	-0.68
Klk8	-0.44	-0.17	0.00	0.46	1.44	-0.57	0.40	0.10	-0.28	-1.91	-1.45	-1.55	0.44	0.40	1.84	0.79	-0.75	0.57
		-	-							-	-	-					<u> </u>	
Scn3b	0.48	0.03	0.51	-0.73	-0.37	-0.17	1.00	0.52	0.58	-1.28	-1.19	-1.69	0.57	2.65	0.21	-0.79	0.17	-0.50
Nrxn2	0.23	1.05	0.91	1.62	0.33	0.79	0.69	1.42	0.30	-1.08	-0.41	-0.60	-0.90	-2.12	-1.29	-0.56	-0.20	-0.20
Pcdh19	0.79	2.01	1.11	0.47	0.27	0.12	0.80	0.45	0.06	-1.85	-0.81	-1.12	0.42	-1.11	-0.48	0.91	-1.20	-0.83
Slc12a5	0.99	0.67	0.99	-0.04	-0.39	0.11	1.12	0.88	0.93	-1.05	-0.84	-1.26	0.30	1.32	0.50	-1.65	-1.29	-1.28
Gabrg2	0.66	0.64	1.47	-0.49	0.53	0.47	-0.50	0.52	0.11	-1.31	-1.53	-1.42	0.94	1.08	1.28	-1.59	-0.48	-0.40
Gal	0.45	0.74	0.98	1.40	-0.13	0.37	0.38	0.72	0.85	-1.28	-0.52	-0.59	-0.17	0.23	-2.61	0.97	-1.14	-0.65
Snap25	1.26	1.50	0.83	0.16	0.46	-0.45	0.65	0.64	0.69	-0.89	-1.65	-1.04	0.36	-0.03	0.97	-1.25	-1.83	-0.39
Kif5a	0.29	0.57	0.82	0.31	0.56	0.13	0.55	1.25	1.25	-0.86	-1.13	-0.28	0.37	1.33	-0.30	-1.83	-1.55	-1.49
Cacna2d1	-0.13	0.98	-0.23	1.06	0.92	1.84	0.93	0.42	0.42	-1.02	-1.53	-1.98	0.45	-0.08	-0.01	-0.17	-0.74	-1.14
Map1b	0.28	0.59	0.37	0.50	0.12	0.09	1.07	0.96	1.33	-0.91	-0.77	-1.37	1.37	-0.46	0.99	-1.29	-1.74	-1.13
Gabra2	1.15	1.43	1.29	0.24	0.35	0.18	0.74	0.70	0.21	-0.90	-1.13	-1.03	0.79	-0.39	0.66	-1.63	-1.60	-1.05
Kcna1	0.67	1.35	1.35	0.78	0.27	1.09	0.27	0.07	0.07	-1.71	-1.41	-0.82	0.78	0.58	0.21	-1.45	-1.14	-0.96
Fgf13	-0.02	0.70	0.41	0.11	1.35	1.34	0.55	1.30	1.12	-1.78	-0.74	-1.55	0.03	-0.90	0.47	-1.35	-0.53	-0.51
Phactr1	-0.29	0.36	0.94	0.55	0.55	1.20	0.47	0.31	1.03	-1.47	-0.77	-2.19	0.39	1.26	0.18	-1.57	-0.82	-0.15
Scg2	1.00	1.61	0.96	0.25	0.95	0.83	0.22	0.09	0.05	-1.48	-1.76	-1.50	0.38	0.32	0.72	-1.16	-0.93	-0.5
Scn2a	0.51	0.80	0.58	0.35	0.09	-0.10	1.44	0.82	0.73	-1.09	-2.06	-1.76	0.45	0.63	0.95	-1.29	-0.78	-0.2
Dnm1	0.91	1.24	0.68	1.67	0.44	1.12	0.45	0.14	0.24	-1.78	-1.57	-1.21	0.17	0.22	-0.26	-1.24	-0.32	-0.9
Sptbn2	0.97	1.82	1.04	0.84	0.39	1.05	0.35	0.75	0.54	-1.28	-1.05	-0.98	-0.21	-0.35	-0.23	-1.12	-1.66	-0.9
Gabra1	0.88	1.19	1.21	0.57	0.48	0.85	0.25	0.41	0.39	-1.12	-1.26	-1.00	0.30	0.46	0.80	-1.94	-1.48	-0.99
Neurod2	1.02	0.47	0.63	0.43	0.48	0.33	0.45	0.85	1.08	-0.91	-1.40	-1.21	0.81	1.10	0.22	-1.86	-1.33	-1.1
Gap43	0.79	0.47	0.03	0.60	0.48	0.33	0.43	0.56	0.51	-0.61	-0.61	-1.10	0.52	0.22	1.07	-1.92	-1.81	-1.61
	0.79	0.90	0.71	0.60	0.40	0.40	U.04	0.50	16.0	-0.01	-0.01	-1.10	0.52	0.22	1.07	-1.82	-1.01	-1.01

Table S2. Genotyping and qRT-PCR primer list and description, Related to STAR Methods

Target	Note	Product Size				
	RIP3_001	CGCTTTAGAAGCCTTCAGGTTGAC	WT 700h = KO 405			
Ripk3-/-	RIP3_002	WT 733bp KO 485 bp				
	RIP3_003	CCAGAGGCCACTTGTGTAGCG	БР			
	R3FL_001	R3FL_001 ACGATGTCTTCTGTCAAGTTATG				
Ripk3 ^{fl/fl}	R3FL_002	CAGTTCTTCACGGCTCAC	WT 300bp LoxP 334bp			
	R3FL_003	TCTGGTAAGGAGGGTCAC	σσταρ			
	ROSA forward	AGCACTTGCTCTCCCAAAGTC	346bp			
Ripk3-	ROSA reverse	CCGACAAAACCGAAAATCTGTGGG	346bb			
2xFV ^{fl/fl}	Transgene forward	CGCTTTAGAAGCCTTCAGGTTGAC	340hn			
	Transgene reverse	GCAGGCTCTGGTGACAAGATTCATGG	349bp			
	Transgene forward	CTCAGCGCTGCCTCAGTCT	300bp			
	Transgene reverse	ansgene reverse GCATCGACCGGTAATGCA				
Syn1 Cre	Internal control forward	CTAGGCCACAGAATTGAAAGATCT	324bp			
	Internal control GTAGGTGGAAATTCTAGCATCATCC reverse		324υρ			
	WT forward	TTGCTAAAGCGCTACATAGGA	WT 04Chm Cma			
Nestin Cre	Common reverse	GCCTTATTGTGGAAGGACTG	WT 246bp Cre 150bp			
	Transgene forward CCTTCCTGAAGCAGTAGAGCA		ТООБР			
	MLKL_001	TATGACCATGGCAACTCACG	W/T 400h = 1/0			
MIkI-/-	MLKL_002 ACCATCTCCCCAAACTGTGA		WT 498bp KO 158bp			
	MLKL_003	ТООБР				
Cxcl10	Forward	GCCGTCATTTTCTGCCTCA				
CXCITO	Reverse	CGTCCTTGCGAGAGGGATC				

Table S3. Primer pool used for *Ripk3* Fluorescent In Situ Hybridization (FISH), Related to STAR Methods

Pool name	Sequence
Ripk3_Ms_B2	TCACAGTTAACATGCTATGTTTATTAAATCATCCAGTAAACCGCC
Ripk3 Ms B2	CCTCGTAAATCCTCATCAAACTTTAAGGAGATGGGTCAAGAGTCA
Ripk3_Ms_B2	GGTCCAACTGTCCTCACAGAATGTTAAATCATCCAGTAAACCGCC
Ripk3_Ms_B2	CCTCGTAAATCCTCATCAAAGAGCTTCAGGAAGTGGCAAGGACTG
Ripk3_Ms_B2	CCAGGTTGCTTAAAACGTGCTTTTTAAATCATCCAGTAAACCGCC
Ripk3_Ms_B2	CCTCGTAAATCCTCATCAAATGCCACGCTGAATGGCACACTTCAG
Ripk3_Ms_B2	GATTCTCTGAAGTCTACTTGTGGAAAAATCATCCAGTAAACCGCC
Ripk3_Ms_B2	CCTCGTAAATCCTCATCAAAGCTGCCAGCCCCTACCCCTGCCGAA
Ripk3_Ms_B2	CATACTTGGCCGAACTTGAGGCAGTAAATCATCCAGTAAACCGCC
Ripk3_Ms_B2	CCTCGTAAATCCTCATCAAATTCTTGGTGGTGCTACCAAGGAGTT
Ripk3_Ms_B2	TCTGCACTTCAGAACAGTTGTTGAAAAATCATCCAGTAAACCGCC
Ripk3_Ms_B2	CCTCGTAAATCCTCATCAAACGAGAGCCGGTGGCCCTGTCATTGG
Ripk3_Ms_B2	TCCAGGGATACCAAGGAGTGCCGTGAAATCATCCAGTAAACCGCC
Ripk3_Ms_B2	CCTCGTAAATCCTCATCAAATTCCATCTCCCTGATTCCTTTGGGG
Ripk3_Ms_B2	GAGTCTCAGTAAAGACTGGCCCAGGAAATCATCCAGTAAACCGCC
Ripk3_Ms_B2	CCTCGTAAATCCTCATCAAATTGTGCCTCTGAAGGGTAAAGTATG
Ripk3_Ms_B2	GAGTGCCAGCCACGGGGTCAGAAGAAAATCATCCAGTAAACCGCC
Ripk3_Ms_B2	CCTCGTAAATCCTCATCAAATCCTTGCTGGTGTGGCAGGCCCAAC
Ripk3_Ms_B2	GTGCTTGCCTCTCAGGACATTTTCCAAATCATCCAGTAAACCGCC
Ripk3_Ms_B2	CCTCGTAAATCCTCATCAAAGAACTGGTCCGGAGGGTTCCTCCAA
Ripk3_Ms_B2	CCAGCATTTTAGAAACCATGGTTTCAAATCATCCAGTAAACCGCC
Ripk3_Ms_B2	CCTCGTAAATCCTCATCAAATCGGGCAATCCATTTCTGTGCCTCT
Ripk3_Ms_B2	CTCTGGCAGACAAGTTTCTGCCGCTAAATCATCCAGTAAACCGCC
Ripk3_Ms_B2	CCTCGTAAATCCTCATCAAATTCTGTGCTGAGACAGATAATGCTT
Ripk3_Ms_B2	CAGCAGCATCTACCTTGTCCTTTACAAATCATCCAGTAAACCGCC
Ripk3_Ms_B2	CCTCGTAAATCCTCATCAAAGATTGTAAACTTCATTGGTTTTTGG
Ripk3_Ms_B2	GGAAGGATGGCCTGTTTTCGGACTGAAATCATCCAGTAAACCGCC
Ripk3_Ms_B2	CCTCGTAAATCCTCATCAAAAACCCCAGCAATGAATCATTAACTC
Ripk3_Ms_B2	CCAAGCCGGGAGTCTCAGGGCTACCAAATCATCCAGTAAACCGCC
Ripk3_Ms_B2	CCTCGTAAATCCTCATCAAAGAGGCAGCTCTGTCAGTGGAGGACG
Ripk3_Ms_B2	CACACACTGTTTCCCGGATTAGTGAAAATCATCCAGTAAACCGCC
Ripk3_Ms_B2	CCTCGTAAATCCTCATCAAATCTTGTCTACCAACTCAGCTTCTCT
Ripk3_Ms_B2	CTGCCCACACGAGGATCCCAAAGCTAAATCATCCAGTAAACCGCC
Ripk3_Ms_B2	CCTCGTAAATCCTCATCAAAAGACATCACTCGCTTTAGAAGCCTT
Ripk3_Ms_B2	CAAATAACAGCTCTGGGTCCAAGTAAAATCATCCAGTAAACCGCC
Ripk3_Ms_B2	CCTCGTAAATCCTCATCAAACTAGGGTGCCCCCAGAGTCCCTGGA
Ripk3_Ms_B2	ATCCTGACCCTGACTGGGACCCTCCAAATCATCCAGTAAACCGCC
Ripk3_Ms_B2	CCTCGTAAATCCTCATCAAAGAAACGTGGACAGGCCAAAATCTGC
Ripk3_Ms_B2	GGAGCTCTGGATCCAGCAGAATGTTAAATCATCCAGTAAACCGCC
Ripk3_Ms_B2	CCTCGTAAATCCTCATCAAAAGGGCTTGAGGTCCCGGTGCAGGAG
Ripk3_Ms_B2	AGCTGTGTAGGTAGCACATCCCCAGAAATCATCCAGTAAACCGCC
Ripk3_Ms_B2	CCTCGTAAATCCTCATCAAACCACTTCCTGCAGCAGGCGACAGAG

Ripk3_Ms_B2	GCCGAGGCACTCGGGTTGCAGCAGAAATCATCCAGTAAACCGCC
Ripk3_Ms_B2	CCTCGTAAATCCTCATCAAACTGCGAGGGAGCCATTCTCCATGAA
Ripk3_Ms_B2	GAGCCTGCCCGGACACGAAGTCCCAAAATCATCCAGTAAACCGCC
Ripk3_Ms_B2	CCTCGTAAATCCTCATCAAAGGAGGTCCTCAGTGACCCCCAGCAG
Ripk3_Ms_B2	TCTCATTACGAAGATTAACCATAGCAAATCATCCAGTAAACCGCC
Ripk3_Ms_B2	CCTCGTAAATCCTCATCAAATCACCTCCCAGGATATCTTCTTCGA
Ripk3_Ms_B2	TGACTGCTACATCATGGTTCCATGTAAATCATCCAGTAAACCGCC
Ripk3_Ms_B2	CCTCGTAAATCCTCATCAAATGTGGTGTGCCCGGAACACGACTCC
Ripk3_Ms_B2	TACCCACAAACTCCAGCTTCTTCAGAAATCATCCAGTAAACCGCC
Ripk3_Ms_B2	CCTCGTAAATCCTCATCAAACTTCACGGCTCACCAGAGGAACCGC
Ripk3_Ms_B2	TAGGCCATAACTTGACAGAAGACATAAATCATCCAGTAAACCGCC
Ripk3_Ms_B2	CCTCGTAAATCCTCATCAAATCGGGAGCTAGCGGCTTCCTGGAGT
Ripk3_Ms_B2	AGACGGAGCTGGAAACCCGACGTCTAAATCATCCAGTAAACCGCC
Ripk3_Ms_B2	CCTCGTAAATCCTCATCAAAGGCTCGGAGTGTGGACTGAGAGGAA
Ripk3_Ms_B2	CAAAGGGAACAATCAGTAGGTCAAGAAATCATCCAGTAAACCGCC
Ripk3_Ms_B2	CCTCGTAAATCCTCATCAAAACGGAGGTTCAGGCCCCGAATTCCG
Ripk3_Ms_B2	GCTCCCCGGACTTTGAATGAGCGAAAATCATCCAGTAAACCGCC
Ripk3_Ms_B2	CCTCGTAAATCCTCATCAAATCACAACTTCCCTTTCAAATAAGAG